J|A|C|S
ARTICLES
Published on Web 09/14/2004

Spectroscopic and Computational Studies of the Azide-Adduct of Manganese Superoxide Dismutase: Definitive Assignment of the Ligand Responsible for the Low-Temperature Thermochromism

Timothy A. Jackson,[†] Anush Karapetian,[‡] Anne-Frances Miller,[‡] and Thomas C. Brunold*,[†]

Contribution from the Department of Chemistry, University of Wisconsin-Madison, Madison Wisconsin 53706 and Department of Chemistry, University of Kentucky, Lexington, Kentucky 40506

Received March 26, 2004; E-mail: Brunold@chem.wisc.edu

Abstract: A variety of spectroscopic and computational techniques have been used to examine the thermochromic transition previously reported for the oxidized state of Mn-dependent superoxide dismutase from *E. coli* in the presence of substrate analog azide (N_3−Mn^{3+}SOD).[Whittaker, M. M.; Whittaker, J. W. *Biochemistry* **1996**, *35*, 6762−6770.] Although previous spectroscopic studies had shown that this thermochromic event corresponds to a change in coordination number of the active-site Mn^{3+} ion from 6 to 5 as temperature is increased, the ligand that dissociates in this conversion had yet to be identified. Through the use of electronic absorption, circular dichroism (CD), and magnetic CD (MCD) spectroscopies, both d→d and ligand-to-metal charge-transfer (LMCT) transition energies have been determined for native Mn^{3+}SOD (possessing a five-coordinate Mn^{3+} center) and Y34F N_3−Mn^{3+}SOD (forming a six-coordinate N_3−Mn^{3+} adduct at all temperatures). These two systems provide well-defined reference points from which to analyze the absorption and CD data obtained for N_3−Mn^{3+}SOD at room temperature (RT). Comparison of excited-state spectroscopic data reveals that Mn^{3+}SOD and RT N_3−Mn^{3+}SOD exhibit virtually identical d→d transition energies, suggesting that these two species possess similar geometric and electronic structures and, thus, that azide does not actually coordinate to the active-site Mn^{3+} ion at RT. However, resonance Raman spectra of both N_3−Mn^{3+}SOD and Y34F N_3−Mn^{3+}SOD at 0 °C exhibit azide-related vibrations, indicating that azide does interact with the active site of the native enzyme at this temperature. To gain further insight into the nature of the azide/Mn^{3+} interaction in RT N_3−Mn^{3+}SOD, several viable active-site models designed to promote either dissociation of coordinated solvent, Asp167, or azide were generated using DFT computations. By utilizing the time-dependent DFT method to predict absorption spectra for these models of RT N_3−Mn^{3+}SOD, we demonstrate that only azide dissociation is consistent with experimental data. Collectively, our spectroscopic and computational data provide evidence that the active site of N_3−Mn^{3+}SOD at RT exists in a dynamic equilibrium, with the azide molecule either hydrogen-bonded to the second-sphere Tyr34 residue or coordinated to the Mn^{3+} ion. These results further highlight the role that second-sphere residues, especially Tyr34, play in tuning substrate (analog)/metal ion interactions.

1. Introduction

Superoxide dismutases (SODs)[1] are a family of enzymes that utilize either an Fe, Mn, Cu/Zn, or Ni cofactor to disproportionate the toxic superoxide radical anion, $O_2^{\cdot -}$, that is produced as a byproduct during photosynthesis and aerobic respiration and also plays a major role in reperfusion injury.[2,3] The Mn-dependent SODs (MnSODs) are present in a variety of prokaryotes and eukaryotes. They are highly homologous to FeSODs but structurally unrelated to Cu/Zn- and NiSODs. X-ray crystallography has been used to determine the structures of MnSODs from a variety of diverse organisms, including humans,[4,5] bacteria (i.e., *Escherichia coli* and the thermophilic

[†] Department of Chemistry, University of Wisconsin-Madison.
[‡] Department of Chemistry, University of Kentucky.

(1) Abbreviations: ADF, Amsterdam density functional; CD, circular dichroism; CT, charge transfer; DFT, density functional theory; DOMO, doubly occupied molecular orbital; EDDM, electron density difference map; EPR, electron paramagnetic resonance; HOMO, highest occupied molecular orbital; INDO/S-CI, intermediate neglect of differential overlap/spectroscopic parametrization − configuration interaction; LMCT, ligand-to-metal charge transfer; LT, low temperature; LUMO, lowest-unoccupied molecular orbital; MCD, magnetic circular dichroism; MO, molecular orbital; NIR, near-infrared; PDB, protein data bank; RR, resonance Raman; RT, room temperature; SDS−PAGE, sodium dodecyl sulfate − polyacrylamide gel electrophoresis; SOD, superoxide dismutase; SOMO, singly occupied molecular orbital; TD, time-dependent; UV, ultraviolet; VTVH, variable-temperature, variable-field; WT, wild type.

(2) (a) Packer, L., Ed.; *Methods in Enzymology: Superoxide Dismutase*; Academic Press: San Diego, 2002; Vol. 349. (b) Miller, A.-F.; Sorkin, D. L. *Comments Mol. Cell. Biophys.* **1997**, *9*, 1−48. (c) Miller, A.-F. In *Comprehensive Coordination Chemistry II*; McCleverty, J. A., Meyer, T. J., Eds.; Elsevier Ltd.: Oxford, UK, 2004; Vol. 8, pp 479−506. (d) Miller, A.-F. *Curr. Opin. Chem. Biol.* **2004**, *8*, 162−168.

(3) Valentine, J. S.; Wertz, D. L.; Lyons, T. J.; Liou, L.; Goto, J. J.; Gralla, E. B. *Curr. Opin. Chem. Biol.* **1998**, *2*, 253−262.

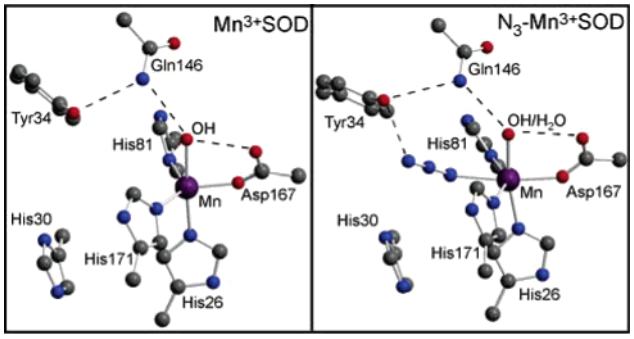

Figure 1. Active-site structures of *E. coli* Mn^{3+}SOD (left) and *T. thermophilus* N_3-Mn^{3+}SOD (right) based on coordinates from the protein data bank files 1VEW and 1MNG-L, respectively. Dashed lines indicate important H-bonding interactions. Note that the *E. coli* amino acid numbering scheme is used for both species.

bacterium *Thermus thermophilus*),[6−14] and a fungus that has been implicated in certain lung diseases.[15] These studies have invariably revealed a distorted trigonal bipyramidal ligand environment around the manganese ion, consisting of two histidines (His81 and His171, using the *E. coli* MnSOD numbering scheme)[16] and an aspartate residue (Asp167) in the equatorial plane and a third histidine residue (His26) and a solvent molecule in the axial positions (Figure 1, left). In addition to these active-site ligands, several second-sphere residues such as Gln146 and Tyr34, which are part of a hydrogen-bonding network involving coordinated solvent and Asp167 (Figure 1, dashed lines), are highly conserved among MnSODs. Experimental and computational studies have suggested that the protonation state of the solvent ligand is coupled to the oxidation state of the metal ion, with the oxidized state coordinating a hydroxide ion and the reduced state binding a water molecule (see eq 1).[17−20] Thus, coordinated solvent may provide one of the two protons required in the two-step catalytic mechanism originally elucidated by Fridovich and co-workers based on pulse radiolysis studies (eq 2).[21]

$$Mn^{3+}SOD^{OH} + e^- + H^+ \rightarrow Mn^{2+}SOD^{H2O} \quad (1)$$

$$Mn^{3+}SOD^{OH} + O_2^{\bullet -} + H^+ \rightarrow Mn^{2+}SOD^{H2O} + O_2 \quad (2a)$$

$$Mn^{2+}SOD^{H2O} + O_2^{\bullet -} + H^+ \rightarrow Mn^{3+}SOD^{OH} + H_2O_2 \quad (2b)$$

Small anions such as azide (N_3^-) and fluoride (F^-) have been frequently used to model substrate/metal ion interactions.[11,12,17,22−25] Studies of Mn^{3+}SODs in the presence of azide (yielding N_3-Mn^{3+}SOD) have shown that these systems exhibit spectroscopic properties that are temperature dependent.[23,24] While a room temperature (RT) X-ray structure of N_3-Mn^{3+}SOD from *T. thermophilus* revealed that N_3^- binding to Mn^{3+}SOD increases the coordination number of the Mn^{3+} center from 5 to 6, generating a distorted octahedral geometry (Figure 1, right),[12] previous studies utilizing RT absorption and circular dichroism (CD) spectroscopies had suggested that azide binding to *E. coli* Mn^{3+}SOD did not expand the coordination sphere of the Mn^{3+} ion.[22] Subsequent variable-temperature spectroscopic studies of N_3-Mn^{3+}SODs from *E. coli* and *T. thermophilus*[23,24] indicated that these species are thermochromic, exhibiting distinct absorption and CD spectra above and below an organism-specific transition temperature (225 and 305 K for the *E. coli* and *T. thermophilus* enzymes, respectively).[23,24] Due to the fact that (i) the low temperature (LT) species exhibits a "red-band" in the absorption spectrum at ~11 000 cm^{-1}, characteristic of six-coordinate Mn^{3+} systems,[26] whereas the lowest-energy band for the high temperature form occurs at ~16 500 cm^{-1}, and (ii) the ΔH for the thermochromic conversion ($\Delta H \approx 5$ kcal/mol) is in the range of bond dissociation enthalpies for Mn^{3+} complexes, it was proposed that the thermochromic event corresponds to a conversion from a six- to a five-coordinate Mn^{3+} ion as temperature is increased.[23,24] Intriguingly, mutagenesis studies of *E. coli* Mn^{3+}SOD have shown that replacement of the second-sphere Tyr34 residue (Figure 1) with Phe followed by treatment of the corresponding variant with azide results in a species (Y34F N_3-Mn^{3+}SOD) that exhibits a temperature-independent absorption spectrum (Figure 2) resembling that of LT N_3-Mn^{3+}SOD,[27] thus suggesting that azide binding to Y34F Mn^{3+}SOD results in the formation of a six-coordinate Mn^{3+} ion at all temperatures. However, the mechanism by which this second-sphere substitution prevents ligand dissociation at RT is currently unclear, and the identity of the ligand that dissociates upon the LT to RT conversion of the native enzyme also remains unknown.

It has generally been assumed that azide dissociation is not responsible for the LT to RT conversion of N_3-Mn^{3+}SOD because the absorption spectrum of the RT form (Figure 2) appears to exhibit $N_3^- \rightarrow Mn^{3+}$ charge-transfer (CT) transitions in the near-UV,[23] though detailed assignments of near-UV spectral features for Mn^{3+}SOD with or without azide have not yet been reported. Consequently, coordinated solvent or Asp167

(4) Børgstahl, G. E. O.; Parge, H. E.; Hickey, M. J.; Beyer, W. F.; Hallewell, R. A.; Tainer, J. A. *Cell* **1992**, *71*, 107−118.
(5) Wagner, U. G.; Pattridge, K. A.; Ludwig, M. L.; Stallings, W. C.; Werber, M. M.; Oefner, C.; Frolow, F.; Sussman, J. L. *Protein Sci.* **1993**, *2*, 814−825.
(6) Edwards, R. A.; Baker, H. M.; Whittaker, M. M.; Whittaker, J. W.; Jameson, G. B.; Baker, E. N. *J. Biol. Inorg. Chem.* **1998**, *3*, 161−171.
(7) Børgstahl, G. E. O.; Pokross, M.; Chehab, R.; Sekher, A.; Snell, E. H. *J. Mol. Biol.* **2000**, *296*, 951−959.
(8) Schmidt, M.; Meier, B.; Parak, F. *J. Biol. Inorg. Chem.* **1996**, *1*, 532−541.
(9) Liao, J.; Li, M.; Liu, M.-Y.; Chang, T.; Le Gall, J.; Gui, L.-L.; Zhang, J.-P.; Liang, D.-C.; Chang, W.-R. *Biochem. Biophys. Res. Comm.* **2002**, *294*, 60−62.
(10) Liao, J.; Liu, M.-Y.; Chang, T.; Li, M.; Le Gall, J.; Gui, L.-L.; Zhang, J.-P.; Jiang, T.; Liang, D.-C.; Chang, W.-R. *J. Struct. Biol.* **2002**, *139*, 171−180.
(11) Ludwig, M. L.; Metzger, A. L.; Pattridge, K. A.; Stallings, W. C. *J. Mol. Biol.* **1991**, *219*, 335−358.
(12) Lah, M. S.; Dixon, M. M.; Pattridge, K. A.; Stallings, W. C.; Fee, J. A.; Ludwig, M. L. *Biochemistry* **1995**, *34*, 1646−1660.
(13) Parker, M. W.; Blake, C. C. *J. Mol. Biol.* **1988**, *199*, 649−171.
(14) Atzenhofer, W.; Regelsberger, G.; Jacob, U.; Peschek, G. A.; Furtmüller, P. G.; Huber, R.; Obinger, C. *J. Mol. Biol.* **2002**, *321*, 479−489.
(15) Flückiger, S.; Mittl, P. R. E.; Scapozza, L.; Fijten, H.; Folkers, G.; Grütter, M. G.; Blaser, K.; Crameri, R. *J. Immunol.* **2002**, *168*, 1267−1272.
(16) The *E. coli* MnSOD amino acid numbering scheme is used in this study unless otherwise indicated.
(17) Stallings, W. C.; Metzger, A. L.; Pattridge, K. A.; Fee, J. A.; Ludwig, M. L. *Free Radic. Res. Commun.* **1991**, *12*−*13*, 259−268.
(18) Tierney, D. L.; Fee, J. A.; Ludwig, M. L.; Penner-Hahn, J. E. *Biochemistry* **1995**, *34*, 1661−1668.
(19) Han, W.-G.; Lovell, T.; Noodleman, L. *Inorg. Chem.* **2002**, *41*, 205−218.
(20) Miller, A. F.; Padmakumar, F.; Sorkin, D.; Karapetian, A.; Vance, C. K. *J. Inorg. Biochem.* **2003**, *93*, 71−83.
(21) Pick, M.; Rabani, J.; Yost, F.; Fridovich, I. *J. Am. Chem. Soc.* **1974**, *96*, 7329−7333.
(22) Whittaker, J.; Whittaker, M. *J. Am. Chem. Soc.* **1991**, *113*, 5528−5540.
(23) Whittaker, M. M.; Whittaker, J. W. *Biochemistry* **1996**, *35*, 6762−6770.
(24) Whittaker, M. M.; Whittaker, J. W. *J. Biol. Inorg. Chem.* **1997**, *2*, 667−671.
(25) Un, S.; Dorlet, P.; Voyard, G.; Tabares, L. C.; Cortez, N. *J. Am. Chem. Soc.* **2001**, *123*, 10 123−10 124.
(26) Lever, A. B. P. *Inorganic Electronic Spectroscopy*, 2nd ed.; Elsevier: Amsterdam; New York, 1984.
(27) Whittaker, M. M.; Whittaker, J. W. *Biochemistry* **1997**, *36*, 8923−8931.

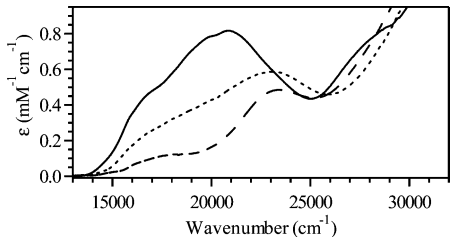

Figure 2. Room-temperature absorption spectra of Mn^{3+}SOD (solid line), N_3-Mn^{3+}SOD (dotted line), and Y34F N_3-Mn^{3+}SOD (dashed line).

have been viewed as the most likely candidates for the dissociating ligand upon conversion from LT to RT N_3-Mn^{3+}-SOD. Support for a model involving Asp167 dissociation is provided by the partial bleaching of the prominent absorption band at ~21 000 cm^{-1} when azide is added to Mn^{3+}SOD at RT (Figure 2). As the d → d transitions of the Mn^{3+} center, which produce the dominant contribution to this band, appear to gain their intensities through mixing with $Asp^- \rightarrow Mn^{3+}$ CT transitions,[28] dissociation of Asp167 should drastically reduce the intensities of these transitions. However, we have recently shown that deprotonation of Tyr34 (Figure 1) also results in slight optical bleaching,[29,30] suggesting that changes in the dielectric environment of the Mn^{3+} ion, which could be caused by the presence of a nearby, but noncoordinating, N_3^- or OH^- molecule, are sufficient to cause a loss of absorption intensity. Furthermore, while the dissociation of Asp167 would essentially eliminate mixing between Mn^{3+} d → d and $Asp^- \rightarrow Mn^{3+}$ CT transitions, the ligation of N_3^- should yield $N_3^- \rightarrow Mn^{3+}$ CT transitions in the near-UV that would provide an alternative intensity source for d → d transitions. Thus, while several models of the five-coordinate form of N_3-Mn^{3+}SOD have been proposed, the rigorous evaluation of these models on the basis of experimental or computational evidence has been lacking.

In this study, a variety of spectroscopic tools were used to explore the electronic properties of resting Mn^{3+}SOD, RT N_3-Mn^{3+}SOD, and Y34F N_3-Mn^{3+}SOD, the last of which provides a six-coordinate N_3-Mn^{3+} adduct that can be studied at room temperature. Additionally, DFT and time-dependent DFT (TD-DFT) computations were employed to assist in the analysis of these spectroscopic data and to allow for the evaluation of possible models of RT N_3-Mn^{3+}SOD on the basis of experimental data. Our results indicate that in RT N_3-Mn^{3+}SOD the azide molecule alternates between two binding sites: (i) H-bonding strongly to Tyr34 and remote from the Mn^{3+} ion, and (ii) directly coordinated to the Mn^{3+} ion, as in LT N_3-Mn^{3+}SOD. Possible implications of these results with respect to the catalytic function of MnSOD are discussed.

2. Materials and Methods

2.1 Sample Preparation. The variant protein Y34F MnSOD was generated by introducing the Y34F mutation in the SodA gene through site-directed mutagenesis using the primer 5′-TTGTTTACAAAG-GTCTGATG-3′. Wild-type (WT) MnSOD and Y34F MnSOD from *E. coli* were purified using an improved version[31] of the normal procedure.[30,32,33] In brief, the ammonium sulfate concentration used in previous procedures was restricted to only 45% saturation and the step that involves heating the crude extract to 60 °C was eliminated. Fractions from all columns were assayed for SOD activity,[34] and only active fractions were carried forward, in contrast to the previous practice of assessing the presence of SOD on the basis of SOD protein content as revealed by SDS-PAGE. Moreover, an additional (third) column was used to achieve higher purity (sephadex A-50, using 5 mM potassium phosphate at pH 7.8 both to preequilibrate and develop the column). This modified procedure resulted in purified WT and Y34F MnSODs with specific activities of ~12 000 units/mg·min and ~9000 units/mg·min, respectively, a drastic improvement over those reported previously (~7000 units/mg·min and ~4800 units/mg·min for WT and Y34F Mn^{3+}SOD, respectively).[30,32,35] Both MnSOD and Y34F MnSOD were isolated predominantly in the oxidized state and were thus not treated with chemical oxidants. The Mn^{3+}SOD species used in this study were ~0.5−5 mM in 50 mM phosphate buffer (pH 7.0).

N_3-Mn^{3+}SOD and Y34F N_3-Mn^{3+}SOD were generated by incubating the resting oxidized enzyme with excess azide (for electronic spectroscopic experiments) or a concentrated solution of azide to ensure complexation of ~95−100% Mn^{3+}SOD active sites with azide (for resonance Raman experiments, as determined by the K_d values for these azide adducts: K_d = 7.2 and 1.6 mM for WT Mn^{3+}SOD and Y34F Mn^{3+}SOD, respectively).[22,27] Azide was not added in excess for resonance Raman experiments in order to avoid possible interference between the signals associated with free and coordinated azide. The exact concentrations of Mn^{3+}SOD and azide used for these experiments are given in the appropriate figure captions.

2.2 Absorption, CD, and MCD Experiments. RT absorption spectra were recorded on a Cary 5E spectrophotometer equipped with near-infrared, visible, and ultraviolet detection capabilities. LT absorption as well as variable-temperature CD and MCD spectra were collected on a spectropolarimeter (Jasco J-715) in conjunction with a magnetocryostat (Oxford Instruments SM-4000) capable of fields up to 8 T. Glycerol, used as a glassing agent in LT spectroscopic experiments, had no effect on the RT CD spectra of Mn^{3+}SOD and Y34F N_3-Mn^{3+}SOD, indicating that this glassing agent does not interact with the Mn^{3+} active site. Typically, LT samples were prepared in 55% (v/v) glycerol and 50 mM phosphate buffer (pH 7.0).

2.3 Resonance Raman Experiments. Resonance Raman (RR) spectra were collected upon excitation with either an Ar^+ (Coherent I-305) or Kr^+ (Coherent I-90) ion laser with incident power in the 5−20 mW range for high-temperature samples and 20−60 mW for LT samples, using a ~135° backscattering arrangement. Samples were kept in NMR tubes that were placed in an EPR dewar. To obtain data at 0 °C (273 K), the EPR dewar was packed with an ice−water mixture, whereas for 77 K experiments the EPR dewar was filled with liquid N_2. The scattered light was dispersed by a triple monochromator (Acton Research, equipped with 300, 1200, and 2400 g/mm gratings) and detected with a back-illuminated CCD camera (Princeton Instruments, 1340 × 100 pixels). Note that while previous RR experiments were hindered by a strong fluorescence background that prevented detection of vibrational modes associated with N_3-Mn^{3+}SOD, the modified purification procedure used for this study[31] resulted not only in higher specific activities but also drastically lowered fluorescence.

A resonance Raman excitation profile was obtained by monitoring the intensity of the peak associated with the symmetric N_3^- stretching mode, $\nu_s(N_3)$, at ~1340 cm^{-1} relative to the intensity of the 984 cm^{-1} mode of sulfate anion that was added to ~25−50 mM in some samples as an internal standard. For 0 °C experiments, sample degradation was monitored via absorption spectroscopy. In the case of visible laser excitation (676−407 nm), absorption data collected before and after

(28) Whittaker, M. M.; Ekberg, C. A.; Edwards, R. A.; Baker, E. N.; Jameson, G. B.; Whittaker, J. W. *J. Phys. Chem. B* **1998**, *102*, 4668−4677.
(29) Jackson, T. A.; Xie, J.; Yikilmaz, E.; Miller, A.-F.; Brunold, T. C. *J. Am. Chem. Soc.* **2002**, *124*, 10 833−10 845.
(30) Maliekal, J.; Karapetian, A.; Vance, C.; Yikilmaz, E.; Wu, Q.; Jackson, T.; Brunold, T. C.; Spiro, T. G.; Miller, A.-F. *J. Am. Chem. Soc.* **2002**, *124*, 15 064−15 075.
(31) Karapetian, A.; Miller, A.-F., unpublished results.
(32) Vance, C. K.; Miller, A.-F. *Biochemistry* **1998**, *37*, 5518−5527.
(33) Slykhouse, T. O.; Fee, J. A. *J. Biol. Chem.* **1976**, *251*, 5472−5477.
(34) Nishikimi, M.; Rao, N.; Jagy, K. *Biochem. Biophys. Res. Comm.* **1972**, *46*, 846−856.

resonance Raman experiments were similar, though the latter were often partially bleached to a varying extent, probably due to photoreduction of the Mn^{3+} center. Experiments performed with UV excitation, on the other hand, did result in sample degradation, as evidenced by the generation of a dark precipitate in the protein solution. Thus, only data collected using visible excitation are presented.

2.3 Computations. (A) Active-Site Models. The active-site model of resting Mn^{3+}SOD and hypothetical active-site models of RT N_3-Mn^{3+}SOD were generated using the PDB file of Mn^{3+}SOD from *E. coli* (1VEW)[6] and N_3-Mn^{3+}SOD from *T. thermophilus* (1MNG-L),[12] respectively. For all models, the Asp and His ligands (Figure 1) were replaced by acetate and 4-methylimidazole, respectively, and the second-sphere Tyr and Gln residues were modeled by 4-methylphenol and acetamide, respectively. As all first sphere amino acid residues were truncated at the C_β positions, the $C_\alpha-C_\beta$ bond was replaced by an $H-C_\beta$ bond of length 1.113 Å; thus, the terminal methyl groups of all first sphere ligands used in our active-site models are referred to as the H_3C_β groups. Hypothetical active-site models for the RT form of N_3-Mn^{3+}-SOD (referred to as N_3-Mn^{3+}SOD($-$OH), N_3-Mn^{3+}SOD($-H_2O$), $N_3-Mn^{3+}SOD^{OH}(-Asp)$, $N_3-Mn^{3+}SOD^{H2O}(-Asp)$, and N_3-Mn^{3+}-$SOD^{OH}(-N_3)$) also included *N*-methylacetamide to model the backbone amide group between Val168 and Trp169 that appears to donate a H-bond to Asp167.[12] For N_3-Mn^{3+}SOD($-$OH) and N_3-Mn^{3+}SOD-($-H_2O$), the axial solvent ligand was positioned such that the oxygen atom of this ligand, O_{sol}, was initially 2.4 Å from the Mn^{3+} ion. For $N_3-Mn^{3+}SOD^{OH}(-Asp)$ and $N_3-Mn^{3+}SOD^{H2O}(-Asp)$ the noncoordinating oxygen atom of the acetate group used to model Asp167, O_{NC}-(Asp167), was protonated, and the C$-$O(Asp167)[36] and C$-O_{NC}$-(Asp167) bond lengths were altered to model C═O double and C$-$O single bonds, respectively. Additionally, the Mn^{3+} ion was moved along the Mn$-$O(Asp167) axis in order to increase the Mn$-$O(Asp167) distance to 2.4 Å. For N_3-Mn^{3+}SOD($-$OH) and $N_3-Mn^{3+}SOD^{OH}(-Asp)$, the H-bond network was altered by moving a proton initially bound to Gln146 halfway between N(Gln146) and O_{sol} and by positioning the phenolic H^+ of Tyr34 in a manner allowing for H-bond donation to N(Gln146). $N_3-Mn^{3+}SOD^{OH}(-N_3)$ was generated by combining the first coordination sphere of resting Mn^{3+}SOD (1VEW) with the second-sphere Tyr34 and Gln146 residues from N_3-Mn^{3+}-SOD (1MNG-L). The positions of the second-sphere residues were determined by superimposing the Mn$-O_{sol}$ and Mn$-$O(Asp167) vectors for 1VEW and 1MNG-L. The azide ligand was positioned within H-bonding distance of the Tyr34 residue ($\sim$1.5 Å) and separated $\sim$3.4 Å from the Mn^{3+} ion. The initial coordinates of all hypothetical active-site models for RT N_3-Mn^{3+}SOD are included as Supporting Information (Tables S2$-$S6).

(B) DFT Geometry Optimizations. Geometry optimizations were performed by fixing the coordinates of the H_3C_β groups of the first-sphere amino acid residues and all atoms of second-sphere residues not involved in the H-bond network (see Figure 1, dotted line). A separate study of LT N_3-Mn^{3+}SOD has shown that this approach allows for a realistic degree of conformational flexibility, while suitably accounting for geometric constraints imposed on the active site by the protein matrix.[37]

Density functional theory (DFT) energy minimizations were performed using the Amsterdam Density Functional (ADF) 2003.01 software package.[38−40] These computations were carried out on a cluster consisting of Intel Xeon processors (Ace Computers) using uncontracted triple-ζ Slater-type orbitals including a single set of polarization functions as the basis set (ADF basis set IV), an integration constant of 3.0 (for geometry optimizations) or 4.0 (for single-point calculations), and the local density approximation of Vosko, Wilk, and Nusair[41] with the nonlocal gradient corrections of Becke[42] and Perdew.[43] Core orbitals were frozen through 1s (O, N, C) and 2p (Mn). All calculations were spin-unrestricted and converged to the $S = 2$ spin state. The coordinates of all DFT energy minimized models presented in this study are included as Supporting Information (Tables S1 and S7$-$S11).

(C) Calculation of Ground and Excited-State Properties. The ORCA 2.2 software package, developed by Dr. Frank Neese,[44] was used to perform semiempirical INDO/S-CI, single point DFT, and time-dependent (TD) DFT calculations on our geometry optimized active-site models. For INDO/S-CI calculations, the ORCA program employs the model of Zerner and co-workers,[45,46] the valence shell ionization potentials and Slater$-$Condon parameters listed by Bacon and Zerner,[47] the standard interaction factors $f_{p\sigma p\sigma} = 1.266$ and $f_{p\pi p\pi} = 0.585$, and the following spin$-$orbit coupling constants: $\zeta_{3d}(Mn) = 300\ cm^{-1}$, $\zeta_{4p}(Mn) = 334\ cm^{-1}$, $\zeta_{2p}(N) = 76\ cm^{-1}$, $\zeta_{2p}(O) = 150\ cm^{-1}$. Restricted open-shell Hartree$-$Fock self-consistent field calculations for our Mn^{3+}-SOD model were tightly converged on the quintet ground state which was used as the reference state for configuration interaction (CI) calculations. Transition energies and intensities were calculated by including single excitations within the 79 highest energy doubly occupied MOs (DOMOs), the 4 singly occupied MOs (SOMOs), and the 80 lowest energy virtual MOs for the quintet states. Ground-state spin Hamiltonian parameters were calculated by including single excitations within the 40 highest energy DOMOs, the 4 SOMOs, and the 26 lowest energy virtual MOs, together with double excitations within the highest 35 DOMOs, the SOMOs, and the 7 lowest energy virtual MOs for the quintet states as well as single electron excitations within the 4 SOMOs for the triplet states. In each case, the completeness of the active space was verified by the insensitivity of the calculated zero-field splitting parameters or excited-state energies to the inclusion of additional one- and two-electron excitations.

For single-point DFT calculations, the SV(P) (Ahlrichs polarized split valence) basis[48,49] with the SV/C auxiliary basis[50] were used for all atoms except Mn, where the larger TZVP (Ahlrichs polarized triple-ζ valence) basis[49,51] in conjunction with the TZV/J auxiliary basis were employed. These computations employed Becke's three-parameter hybrid functional for exchange[52,53] combined with the Lee$-$Yang$-$Parr correlation functional[54] (B3LYP/G), using the default 20% Hartree$-$Fock exchange. The size of the integration grid used for all calculations was 3 (Lebedev 194 points). Isosurface plots of natural orbitals were generated by the gOpenMol program developed by Laaksonen[55,56] using an isodensity value of 0.03 b^{-3}.

Electronic excitation energies and absorption intensities for all Mn^{3+} active-site models used in this study were also determined by the TD-

(35) Vance, C. K.; Miller, A.-F. *J. Am. Chem. Soc.* **1998**, *120*, 461−467.
(36) O(Asp167) and O_{NC}(Asp167) refer to the coordinating and noncoordinating oxygen atoms, respectively, of the acetate group used to model Asp167.
(37) Jackson, T. A.; Karapetian, A.; Miller, A.-F.; Brunold, T. C., manuscript in preparation.
(38) te Velde, G.; Bickelhaupt, F. M.; van Gisbergen, S. J. A.; Guerra, C. F.; Baerends, E. J.; Snijders, J. G.; Ziegler, T. *J. Comput. Chem.* **2001**, *22*, 931−967.
(39) Guerra, C. F.; Snijders, J. G.; te Velde, G.; Baerends, E. J. *Theor. Chem. Acc.* **1998**, *99*, 391−403.
(40) ADF2003.01, SCM, Theoretical Chemistry, Vrije Universiteit, Amsterdam, The Netherlands, http://www.scm.com.
(41) Vosko, S. H.; Wilk, L.; Nusair, M. *Can. J. Phys.* **1980**, *58*, 1200.
(42) Becke, A. D. *J. Chem. Phys.* **1986**, *84*, 4524−4529.
(43) Perdew, J. P. *Phys. Rev. B* **1986**, *33*, 8822−8824.
(44) Neese, F. *ORCA − an ab initio, Density Functional and Semiempirical Program Package, Version 2.2*, Max Planck Institut für Strahlenchemie, Mülheim, 2002.
(45) Ridley, J.; Zerner, M. C. *Theor. Chim. Acta* **1973**, *32*, 111.
(46) Zerner, M. C.; Loew, G. H.; Kirchner, R. F.; Mueller-Westerhof, U. T. *J. Am. Chem. Soc.* **1980**, *102*, 589.
(47) Bacon, A. D.; Zerner, M. C. *Theor. Chim. Acta* **1979**, *53*, 21.
(48) Schäfer, A.; Horn, H.; Ahlrichs, R. *J. Chem. Phys.* **1992**, *97*, 2571−2577.
(49) Ahlrichs, R., unpublished results.
(50) The Ahlrichs auxiliary basis sets were obtained from the TurboMole basis set library under ftp.chemie.uni-karlsruhe.de/pub/cbasen. Weigend, F.; Häser, M. *Theor. Chem. Acc.* **1997**, *97*, 331−340.
(51) Schäfer, G.; Horn, H.; Ahlrichs, R. *J. Chem. Phys.* **1994**, *100*, 5829−5835.
(52) Becke, A. D. *J. Chem. Phys.* **1993**, *98*, 1372−1377.
(53) Becke, A. D. *J. Chem. Phys.* **1993**, *98*, 5648−5652.
(54) Lee, C.; Yang, W.; Parr, R. G. *Phys. Rev. B* **1988**, *37*, 785−789.
(55) Laaksonen, L. *J. Mol. Graphics* **1992**, *10*, 33−34.
(56) Bergman, D. L.; Laaksonen, L.; Laaksonen, A. *J. Mol. Graphics & Modelling* **1997**, *15*, 301−306.

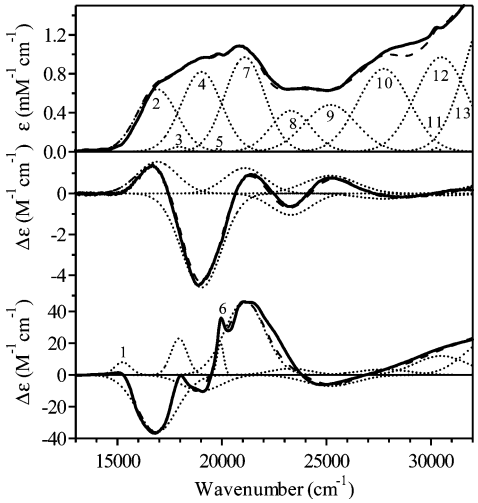

Figure 3. 10 K electronic absorption (top), 4.5 K CD (center), and 4.5 K, 7 T MCD (bottom) spectra of Mn^{3+}SOD. Individual Gaussian curves (dotted lines) and their sums (dashed lines) obtained from iterative fits of these data sets are displayed on their respective spectra. Conditions: 3 mM Mn^{3+}-SOD in 50 mM phosphate buffer (pH 7.0) and 50% (v/v) glycerol.

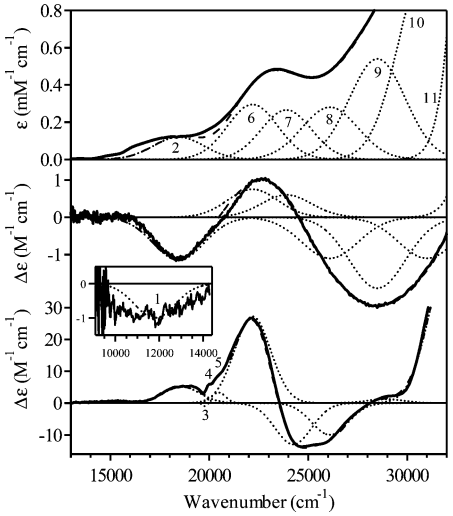

Figure 4. Room-temperature electronic absorption (top), CD (center), and 4.5 K, 7 T MCD (bottom) spectra of Y34F N_3−Mn^{3+}SOD. The near-IR region of the MCD spectrum is shown on an expanded scale in the inset. Individual Gaussian curves (dotted lines) and their sums (dashed lines) obtained from iterative fits of these data sets are displayed on their respective spectra. Conditions: 2.0 mM Y34F Mn^{3+}SOD and 180 mM NaN_3 in 50 mM phosphate buffer (pH 7.0) and, for MCD data, 55% (v/v) glycerol.

DFT[57−59] method within the Tamm−Dancoff approximation,[60,61] employing the B3LYP/G hybrid functional and the basis sets described above. The resolution of the identity approximation in calculating the Coulomb term[62] was used to ensure convergence of all TD-DFT calculations. In each case, 40 excited states were calculated by including all one-electron excitations within an energy window of ± 3 hartrees with respect to the HOMO/LUMO energies. Isosurface plots of electron density difference maps (EDDMs) were generated with the gOpenMol program[55,56] using an isodensity value of 0.003 b^{-3}.

3. Results and Analysis

3.1 Electronic Spectroscopy. (A). WT Mn^{3+}SOD. Our LT absorption, CD, and MCD data collected for Mn^{3+}SOD shown in Figure 3 are virtually identical to those published previously.[22,23,28,29,63] Using the d → d transition energies determined by polarized single-crystal absorption studies of RT Mn^{3+}SOD as a starting point,[28] iterative Gaussian fitting of our absorption, CD, and MCD spectra reveals that at least 13 transitions contribute to the spectral region between 14 000 and 33 000 cm^{-1} (Figure 3, Table S12). On the basis of their energetic positions and relatively moderate widths, and supported by previous assignments,[22,28] bands 2, 4, 7, and 8, which give rise to the broad absorption envelope in the visible region, are assigned as the four spin-allowed Mn^{3+} d → d transitions expected for this $3d^4$ ion. As these d → d transitions are formally symmetry forbidden, their moderate intensities likely reflect significant mixing with intense ligand-to-metal charge-transfer (LMCT) transitions that occur at higher energies. Because the d → d transitions are polarized roughly along the Mn−O(Asp167) axis, it has been proposed that they gain their absorption intensities primarily through mixing with Asp^- → Mn^{3+} CT transitions.[28] Bands 1, 3, 5, 6, and 11, which contribute negligibly to the absorption spectrum and are significantly narrower than the bands associated with the spin-allowed d → d transitions, are assigned as spin-forbidden quintet to triplet d → d (i.e., spin-flip) transitions of the Mn^{3+} ion.

Bands 9, 10, 12, and 13 are generally broader and less intense in the CD and MCD spectra than the d → d bands and are thus assigned as LMCT transitions. The presence of LMCT transitions in the visible to near-UV region is not unusual for a Mn^{3+} species[26] and reflects the moderately high reduction potential of the Mn^{3+} ion. While in Mn^{3+}SOD the reduction potential of the Mn^{3+} ion is greatly depressed from its free ion value by the protein matrix,[35,64] this redox-tuning is largely achieved by disfavoring the protonation of the solvent ligand upon reduction.[65] As the formal reduction of the Mn^{3+} ion accompanying a LMCT excitation is too rapid to allow for protonation of the solvent ligand, the LMCT energies of Mn^{3+}SOD should indeed reflect a typical Mn^{3+} species. Overall, our analysis of absorption, CD, and MCD spectra obtained for Mn^{3+}SOD is consistent with, but more complete than, previous analyses that focused mainly on the d → d region. Importantly, our analysis provides both d → d and LMCT transition energies and intensities, providing an excellent framework within which to interpret spectroscopic data of RT N_3−Mn^{3+}SOD.

(B). Y34F N_3−Mn^{3+}SOD. While the absorption, CD, and MCD spectra of Y34F Mn^{3+}SOD in the absence of azide are virtually identical to those of WT Mn^{3+}SOD (cf., Figures 3 and S1), the addition of azide greatly perturbs the spectroscopic properties of this variant protein at both RT and LT (Figure 4). Most significantly, the LT MCD spectra of Y34F N_3−Mn^{3+}-SOD exhibits a weak, negative band in the NIR (∼11 000 cm^{-1}) that has no counterpart in the MCD spectrum of Mn^{3+}SOD, where the lowest energy feature is observed at ∼16 000 cm^{-1}.

(57) Bauernschmitt, R.; Ahlrichs, R. *Chem. Phys. Lett.* **1996**, *256*, 454−464.
(58) Casida, E. M.; Jamorski, C.; Casida, K. C.; Salahub, D. R. *J. Chem. Phys.* **1998**, *108*, 4439−4449.
(59) Stratman, R. E.; Scuseria, G. E.; Frisch, M. J. *J. Chem. Phys.* **1998**, *109*, 8218−8224.
(60) Hirata, S.; Head-Gordon, M. *Chem. Phys. Lett.* **1999**, *302*, 375−382.
(61) Hirata, S.; Head-Gordon, M. *Chem. Phys. Lett.* **1999**, *314*, 291−299.
(62) Neese, F.; Olbrich, G. *Chem. Phys. Lett.* **2002**, *362*, 170−178.
(63) The increase in absorption intensity upon cooling, $\epsilon(20\,920\ cm^{-1}) = 850\ M^{-1}cm^{-1}$ at RT versus $\epsilon(20\,920\ cm^{-1}) = 1080\ M^{-1}cm^{-1}$ at 10 K, is consistent with previous VT absorption studies performed for this system (see ref 22).
(64) Vance, C. K.; Miller, A. F. *Biochemistry* **2001**, *40*, 13 079−13 087.
(65) (a) Yikilmaz, E.; Xie, J.; Brunold, T. C.; Miller, A.-F. *J. Am. Chem. Soc.* **2002**, *124*, 3482−3483. (b) Schwartz, A. L.; Yikilmaz, E.; Vance, C. K.; Vathyam, S.; Miller, A.-F. *J. Inorg. Biochem.* **2000**, *80*, 247−256.

These data suggest that the electronic and, thus, the geometric structuresof Y34F N_3−Mn^{3+}SOD are greatly different from those of resting Mn^{3+}SOD.

A Gaussian deconvolution of the absorption, CD, and MCD spectra of Y34F N_3−Mn^{3+}SOD reveals the presence of at least 11 transitions that span the NIR to the near-UV spectral region (Figure 4). On the basis of their absorption and MCD intensities as well as their moderate widths, bands 1, 2, 6, and 7 are assigned as the four spin-allowed d → d transitions. The drastic red-shifting of the lowest-energy, spin-allowed d → d transition of Y34F N_3−Mn^{3+}SOD (band 1) relative to Mn^{3+}SOD (band 2, see Figure 3) is indicative of the formation of a six-coordinate Mn^{3+} center upon the addition of azide to Y34F Mn^{3+}SOD. Bands 3−5, based on their sharpness and lack of appreciable absorption intensity, are assigned as spin-forbidden, spin-flip transitions of the Mn^{3+} center, whereas bands 8 through 11, which carry substantial absorption intensity but relatively minor MCD intensity, are assigned as LMCT transitions. By analogy to N_3−Fe^{3+}SOD[66] and the LT form of N_3−Mn^{3+}SOD,[37] the ligand most likely involved in these LMCT transitions is azide.

As both the spin-allowed and spin-forbidden d → d transition energies observed for Y34F N_3−Mn^{3+}SOD are very similar to those determined for LT N_3−Mn^{3+}SOD[37] (Table S13), the ligand environment of the Mn^{3+} center must be nearly identical in these two species. Moreover, the LMCT transition energies are also rather similar, although the two transitions responsible for bands 9 and 10 in the LT N_3−Mn^{3+}SOD spectra (Table S13) are unresolved in the spectra of Y34F N_3−Mn^{3+}SOD. This small difference in the LMCT region between these two species is not surprising considering that the substitution of Tyr34 to Phe eliminates the putative H-bond between the second-sphere Tyr34 residue and the azide ligand (Figure 1, right). The elimination of this H-bond is expected to alter the energies of the azide frontier orbitals and, therefore, the N_3^- → Mn^{3+} CT transition energies. Nonetheless, our analysis clearly indicates that Y34F N_3−Mn^{3+}SOD and LT N_3−Mn^{3+}SOD have very similar spectroscopic properties and thus likely possess virtually identical active-site structures, as proposed previously on the basis of qualitative considerations.[27] Consequently, Y34F N_3−Mn^{3+}SOD provides a suitable model of the six-coordinate form of N_3−Mn^{3+}SOD that, however, may be studied at RT.

(C) Five-Coordinate N_3−Mn^{3+}SOD. RT absorption and CD data collected for N_3−Mn^{3+}SOD are shown in Figure 5. The absorption spectrum is strikingly similar to that of resting Mn^{3+}-SOD (Figure 3), consisting of a broad feature in the visible region with a shoulder on its lower energy side and more intense features in the near-UV region (∼30 000 cm^{-1}). While previous absorption and CD studies suggested that the broad absorption envelope can be fit with four Gaussian bands corresponding to the four spin-allowed d → d transitions of the Mn^{3+} ion,[23] our analysis of the visible region of the CD spectrum (∼15 000−27 000 cm^{-1}) reveals that at least five transitions actually contribute to this region (see Figure 5, bottom and Table S14).[67] Collectively, our Gaussian deconvolutions of the RT absorption and CD spectra of N_3−Mn^{3+}SOD (Table S14) reveal the presence of four bands of comparable widths in the visible region (bands 1−4) and at least three broader features in the near-UV (bands 5−7).

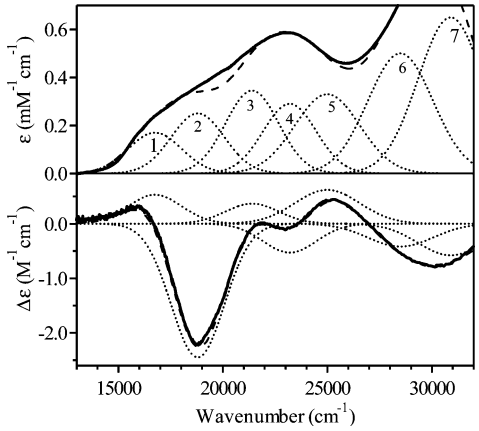

Figure 5. Room-temperature electronic absorption (top) and CD (bottom) spectra of N_3−Mn^{3+}SOD. Individual Gaussian curves (dotted lines) and their sums (dashed lines) obtained from iterative fits of these data sets are displayed on their respective spectra. Conditions: 2.0 mM Mn^{3+}SOD and 180 mM NaN_3 in 50 mM phosphate buffer (pH 7.0).

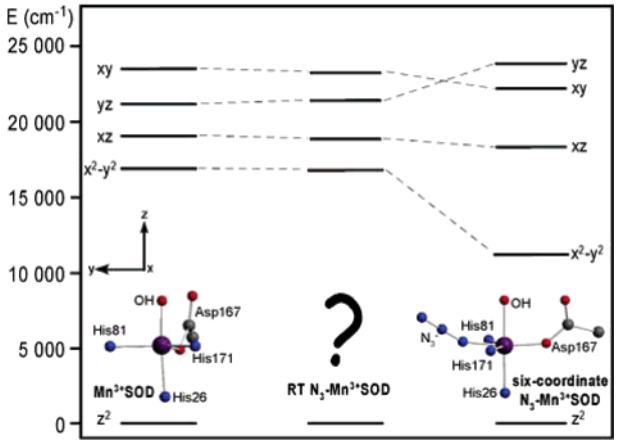

Figure 6. Experimentally determined energies of d → d excited states for Mn^{3+}SOD, RT N_3−Mn^{3+}SOD, and six-coordinate Y34F N_3−Mn^{3+}SOD (states are designated using the hole formalism). The coordinate system relates to the **D**-tensor orientation obtained from INDO/S-CI computations for Mn^{3+}SOD and six-coordinate N_3−Mn^{3+}SOD.

As previously noted by Whittaker and co-workers,[23,24] the d → d transition energies of N_3−Mn^{3+}SOD at RT are suggestive of a five-coordinate active site, since six-coordinate Mn^{3+} complexes invariably exhibit one d → d transition in the near-IR region.[26] Indeed, inspection of our experimentally derived d → d excited-state correlation diagram for resting Mn^{3+}SOD, RT N_3−Mn^{3+}SOD, and the temperature-independent Y34F N_3−Mn^{3+}SOD azide-adduct (Figure 6) reveals remarkable similarities between the former two but drastic differences between the two azide-treated proteins. The relative energies of the d → d excited states shift by at most ∼300 cm^{-1} upon the addition of azide to Mn^{3+}SOD at RT, suggesting that the coordination geometry of RT N_3−MnSOD is, in fact, remarkably similar to the trigonal bipyramidal geometry of resting Mn^{3+}SOD. Others have reported that azide must coordinate to the Mn^{3+} ion at RT, as the near-UV region changes upon the addition of azide due to the appearance of N_3^- → Mn^{3+} CT transitions in this spectral region.[23] However, our Gaussian deconvolution of the RT absorption spectrum of resting Mn^{3+}SOD (Figure S2, Table

(66) Xie, J.; Yikilmaz, E.; Miller, A. F.; Brunold, T. *J. Am. Chem. Soc.* **2002**, *124*, 3769−3774.

(67) While in a previous study the absorption spectrum of RT N_3−Mn^{3+}SOD was fit without a band at ∼21 500 cm^{-1} (see ref 23), our analysis of the CD spectrum of RT N_3−Mn^{3+}SOD clearly requires the presence of a positive Gaussian band at ∼21 500 cm^{-1} (band 3) to achieve satisfactory agreement between the simulated and experimental spectra.

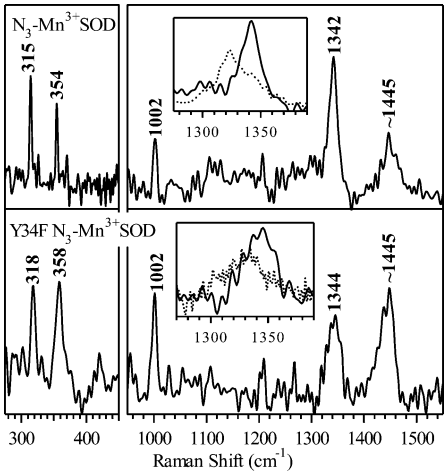

Figure 7. Resonance Raman spectra at 0 °C of N_3-Mn^{3+}SOD and Y34F N_3-Mn^{3+}SOD using 466 nm (21 459 cm^{-1}) excitation. Inset: Expanded view of the $\nu_s(N_3)$ feature for samples prepared with $^{14}N_3$ (solid line) and $^{15}N-^{14}N_2$ (dotted line). Conditions for N_3-Mn^{3+}SOD: 2.6 mM Mn^{3+}SOD and 56 mM NaN_3 in 50 mM phosphate buffer (pH 7.0). Conditions for Y34F N_3-Mn^{3+}SOD: 4.3 mM Y34F Mn^{3+}SOD and 25 mM NaN_3 in 50 mM phosphate buffer (pH 7.0).

S15)[68] reveals that the intensities of the near-UV CT transitions of Mn^{3+}SOD ($f_{exp} \approx 11 \times 10^{-3}$ for band 12) and N_3-Mn^{3+}-SOD ($f_{exp} \approx 9.1 \times 10^{-3}$ for band 7) are actually very similar. Collectively, the minor spectral changes in the NIR/visible/near-UV regions that accompany conversion of Mn^{3+}SOD to N_3-Mn^{3+}SOD at RT suggest that azide does not coordinate directly to the active-site metal ion at RT.

3.2 Resonance Raman Spectroscopy. To further characterize the active site of RT N_3-Mn^{3+}SOD, resonance Raman (RR) spectroscopy was utilized as a selective probe of metal−ligand vibrations. For these experiments the N_3-Mn^{3+}SOD sample was cooled with ice water (~0 °C, 273 K) during data collection so as to minimize photoinduced sample degradation while ensuring that the majority of Mn^{3+} active sites were in the five-coordinate form (at 273 K, $K_{eq} = 6.3$ in favor of the RT species[23]). To interpret RR data obtained for this structurally ill-defined species, parallel experiments were performed on Y34F N_3-Mn^{3+}SOD, a model of the LT, six-coordinate form of N_3-Mn^{3+}-SOD that can be studied at RT.[69]

RR spectra of N_3-Mn^{3+}SOD and Y34F N_3-Mn^{3+}SOD obtained at 0 °C with 466 nm (21 459 cm^{-1}) excitation reveal the presence of five prominent features (Figure 7 and Table 1). Based on RR studies of N_3-Mn^{3+} porphyrins,[70] as many as four features associated with the N_3-Mn^{3+} unit are anticipated in RR spectra of N_3-Mn^{3+} systems; namely, the Mn−N(N_2) stretch, ν(Mn−N), at ~350 cm^{-1}, the N_3^- bend, $\delta(N_3)$, at ~630 cm^{-1}, the symmetric azide stretch, $\nu_s(N_3)$, at ~1320 cm^{-1}, and the antisymmetric azide stretch, $\nu_{as}(N_3)$, at ~2040 cm^{-1}. By analogy, the RR features of N_3-Mn^{3+}SOD and Y34F N_3-Mn^{3+}SOD that occur at ~350 and 1340 cm^{-1} are therefore assigned as ν(Mn−N) and $\nu_s(N_3)$, respectively. Consistent with

Table 1. Peak Positions (cm^{-1}) of the Azide-Related RR Features of Wild-Type (WT) and Y34F N_3-Mn^{3+}SOD at 273 K (0 °C) and 77 K (−196° C)

N_3–MnSOD species	azide isotope	ν(Mn–N_3)	$\nu_s(N_3)$
WT (273 K)	$^{14}N_3$	315; 354	1342
	$^{15}N-^{14}N_2$	ND	1323; 1343
WT (77 K)	$^{14}N_3$	ND	1342
Y34F (273 K)	$^{14}N_3$	318; 358	1344
	$^{15}N-^{14}N_2$	ND	1320; 1342
Y34F (77 K)	$^{14}N_3$	ND	1343

the assignment of the feature at ~1340 cm^{-1} as $\nu_s(N_3)$, this peak broadens and shifts to lower energy when terminally labeled $^{15}N-^{14}N_2$ is used instead of $^{14}N_3$ (Figure 7, insets and Table 1). While the ν(Mn−N) vibration is also expected to show slight isotopic sensitivity (a shift of ~3 cm^{-1}),[70] the low intensity of the RR feature at ~350 cm^{-1} prevented a conclusive analysis of its isotopic behavior. However, as both the energy and width of this low frequency band are sensitive to substitution of Tyr34 (cf. Figure 7, top and bottom), a residue proposed to interact with the azide ligand (Figure 1, right), this feature can safely be attributed to the N_3-Mn^{3+} unit. Similarly, as the width and energy of the band at ~320 cm^{-1} are altered by substitution of Tyr34, this band is assigned as a further component of ν(Mn−N). The presence of more than one feature associated with the Mn−N(N_2) stretching mode suggests that this vibration is coupled with other vibrational modes. It is interesting to note that such coupling was also observed for N_3-Fe^{3+}SOD, where a total of three closely spaced bands were observed between 355 and 380 cm^{-1}.[66] Despite the fact that features at ~630 or 2040 cm^{-1}, corresponding to $\delta(N_3)$ or $\nu_{as}(N_3)$, respectively, could potentially also appear in the RR spectra of N_3-Mn^{3+}-SOD and Y34F N_3-Mn^{3+}SOD, no such features were actually observed, suggesting that excited-state distortions along these coordinates are negligible. The remaining RR features at 1002 and ~1445 cm^{-1} are characteristic of amino acid vibrations[71,72] and are thus not believed to be directly associated with the protein active site. In support of this conclusion, RR excitation profile data show that the band at ~1002 cm^{-1} is not resonance enhanced in the visible spectral region (Figure S3).

It is interesting to note that all vibrations associated with the N_3-Mn^{3+} moiety are considerably sharper for N_3-Mn^{3+}SOD than for Y34F N_3-Mn^{3+}SOD (Figure 7). This difference possibly reflects the loss of a H-bond between Tyr34 and azide in the Y34F variant protein. In the WT protein, this H-bond may stabilize the N_3-Mn^{3+} unit in a single configuration, thus producing relatively sharp RR features. Alternatively, in the Y34F variant, the N_3-Mn^{3+} unit may sample more conformational space, giving rise to a sizable frequency distribution for vibrations associated with the N_3-Mn^{3+} moiety and thus broader RR features.

RR experiments for N_3-Mn^{3+}SOD and Y34F N_3-Mn^{3+}SOD were also performed at 77 K. For these experiments, however, laser excitation typically generated a strong fluorescence background, such that no vibrations associated with the protein samples were detectable at excitation wavelengths >413 nm (<24 207 cm^{-1}). Nonetheless, RR spectra of LT N_3-Mn^{3+}-SOD and Y34F N_3-Mn^{3+}SOD obtained with 413 nm excitation

(68) Here, we have used the RT data for Mn^{3+}SOD (Figure S2) rather than the LT data presented in Figure 3 to permit a meaningful comparison of oscillator strengths, which are weakly temperature dependent, between resting Mn^{3+}SOD and RT N_3-Mn^{3+}SOD.
(69) All RR data were collected using excitation energies below 25 000 cm^{-1}, where LT N_3-Mn^{3+}SOD and Y34F N_3-Mn^{3+}SOD are spectroscopically indistinguishable (see Table S13).
(70) Czernuszewicz, R. S.; Wagner, W.-D.; Ray, G. B.; Nakamoto, K. *J. Mol. Struct.* 1991, *242*, 99−117.
(71) Overman, S. A.; Thomas, G. J. J. *Biochemistry* **1995**, *34*, 5440−5451.
(72) Overman, S. A.; Thomas, G. J. J. *Biochemistry* **1999**, *38*, 4018−4027.

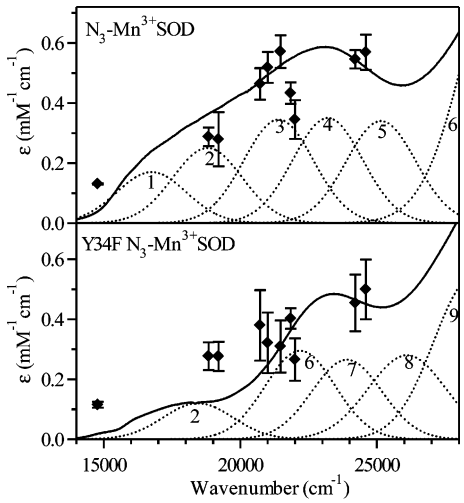

Figure 8. Superposition of room-temperature electronic absorption spectra, Gaussian deconvolutions, and 0 °C resonance Raman excitation profiles of the $\nu_s(N_3)$ vibration (◆) for $N_3-Mn^{3+}SOD$ (top) and Y34F N_3-Mn^{3+}-SOD (bottom). Error bars indicate two standard deviations from three experiments. Conditions are similar to those given in the caption of Figure 7.

permitted observation of the $\nu_s(N_3)$ feature (Figure S4), which, for both systems, appeared at nearly the same frequency as in RR spectra at 273 K (Table 1). This result suggests that the N_3-Mn^{3+} units for the high and low temperature forms of $N_3-Mn^{3+}SOD$ are similar in nature.

Figure 8 compares the RR enhancement behavior of $\nu_s(N_3)$ at 0 °C with the Gaussian deconvoluted absorption spectra of RT $N_3-Mn^{3+}SOD$ (top) and Y34F $N_3-Mn^{3+}SOD$ (bottom). The resonance enhancement behavior of these two species are, within experimental error, identical. In both cases, excitation in resonance with the d → d transitions in the visible region gives rise to considerable enhancement of $\nu_s(N_3)$. Typically, d → d transitions involve rearrangement of electron density predominantly at the metal center; therefore, excitation in resonance with Mn^{3+} d → d transitions (i.e., bands 6 and 7 of Y34F $N_3-Mn^{3+}SOD$) would not necessarily be expected to give rise to enhancement of N_3-Mn^{3+} vibrations. Thus, the RR behavior of $\nu_s(N_3)$ provides direct evidence for strong mixing between these d → d transitions and $N_3^- \rightarrow Mn^{3+}$ CT transitions. Unfortunately, laser excitation at energies >25 000 cm^{-1} resulted in sample degradation, thereby preventing RR-assisted band assignments for near-UV transitions. Thus, while our RR data clearly demonstrate that excitation into the visible absorption band of $N_3-Mn^{3+}SOD$ at 0 °C gives rise to sizable enhancement of vibrational modes associated with the N_3-Mn^{3+} unit, they do not provide evidence for or against the presence of $N_3^- \rightarrow Mn^{3+}$ CT transitions in the near-UV region of the RT $N_3-Mn^{3+}SOD$ or Y34F $N_3-Mn^{3+}SOD$ absorption spectra.

In summary, while absorption and CD data of RT N_3-Mn^{3+}-SOD suggest that azide does not directly coordinate to the active-site Mn^{3+} ion, our RR data provide compelling evidence that azide does in fact associate with the Mn^{3+} center at 273 K. Taken together, these seemingly disparate results do not permit direct identification of the ligand that dissociates upon conversion from LT to RT $N_3-Mn^{3+}SOD$. Nonetheless, these data provide an extensive experimental framework within which this issue can be explored computationally.

3.3 Computations. (A) Resting $Mn^{3+}SOD$. An active-site model of resting $Mn^{3+}SOD$ was generated using the X-ray structure coordinates (PDB file 1VEW)[6] of the first shell ligands, Tyr34, and Gln146 (Figure 1, left). This model was subsequently refined by performing a constrained DFT energy minimization in which the positions of the H_3C_β groups of the first-sphere amino acid residues as well as all coordinates of second-sphere residues except for the H atoms involved in the H-bond network were held fixed. In this optimization process, all metal−ligand bond distances shortened, particularly the $Mn-O_{sol}$ bond length, which decreased from 2.2 to 1.8 Å. This finding is consistent with previous computational studies by Whittaker et al.[28,73] as well as Noodleman and co-workers,[19,74] further validating the assumption that differences in experimental and calculated bond distances may be attributed to redox heterogeneity of the MnSOD crystals used for X-ray structure determination.[28,74] The shortening of the $Mn-O_{sol}$ and Mn−N(His26) bond lengths leads to a compressed Jahn−Teller axis for this system, greatly destabilizing the Mn $3d_z^2$-derived MO relative to the other four Mn 3d-based MOs and, thus, giving rise to a $3d_z^2$ orbital ground state (using the generally adopted hole formalism).

To validate our $Mn^{3+}SOD$ model, INDO/S-CI calculations, shown to be very reliable and reasonably accurate at predicting zero-field splitting parameters for inorganic systems,[75] were performed to predict ground state properties that could be compared directly with experimental results. These computations predict $D = 1.46$ cm^{-1} and $E/D = 0.019$, in reasonable agreement with EPR data ($D = 2.11$ cm^{-1}, $E/D = 0.11$).[76] Consistent with the distorted trigonal bipyramidal active-site geometry, INDO/S-CI calculations predict that the *z*-axis of the **D**-tensor coincides with the $O_{sol}-Mn-N(His26)$ axis, while the *y*-axis is oriented roughly along the Mn−N(His81) bond vector (Figure 9, bottom inset). Knowledge of the **D**-tensor orientation for this system is important as it allows transition polarizations obtained from an analysis of VTVH MCD data[37] to be related to the molecular structure (vide infra).

As a means of further validating our model of $Mn^{3+}SOD$, INDO/S-CI calculations were performed to predict the corresponding electronic absorption spectrum. To facilitate comparison with spectroscopic data, the computed transition energies and oscillator strengths were used to simulate absorption spectra.[77] Comparison of experimental and INDO/S-CI calculated absorption spectra for $Mn^{3+}SOD$ (Figure 9) reveals that the computed d → d transition energies and intensities are fairly accurate, consistent with our previous work on $Mn^{3+}SOD$.[29] However, the INDO/S-CI calculation fails to predict LMCT transitions below ~39 000 cm^{-1}, in clear disagreement with experimental data (Figure 9). This discrepancy between experimental and predicted transition energies using the INDO/S-CI method most likely reflects the propensity of this computational method to overestimate the ionic contributions to metal−ligand bonding, placing the metal d orbitals too high in energy relative

(73) Whittaker, J. *Int. J. Quantum Chem.* **2002**, *90*, 15 629−15 635.
(74) Li, J.; Fisher, C. L.; Konecny, R.; Lovell, T.; Bashford, D.; Noodleman, L. *Inorg. Chem.* **1999**, *38*, 929−939.
(75) Neese, F. *Curr. Opin. Chem. Biol.* **2003**, *7*, 125−135.
(76) Campbell, K. A.; Yikilmaz, E.; Grant, C. V.; Gregor, W.; Miller, A.-F.; Britt, R. D. *J. Am. Chem. Soc.* **1999**, *121*, 4714−4715.
(77) For these simulations it was assumed that each electronic transition may be described by a Gaussian band with a full width at half-maximum ($\nu_{1/2}$) of 3 000 cm^{-1}, in which case the oscillator strength (f_{calc}) of the electronic transition is related to its molar extinction coefficient ϵ_{max} ($M^{-1}cm^{-1}$) by $f_{calc} = 4.61 \times 10^{-9}\ \epsilon_{max}\ \nu_{1/2}$.

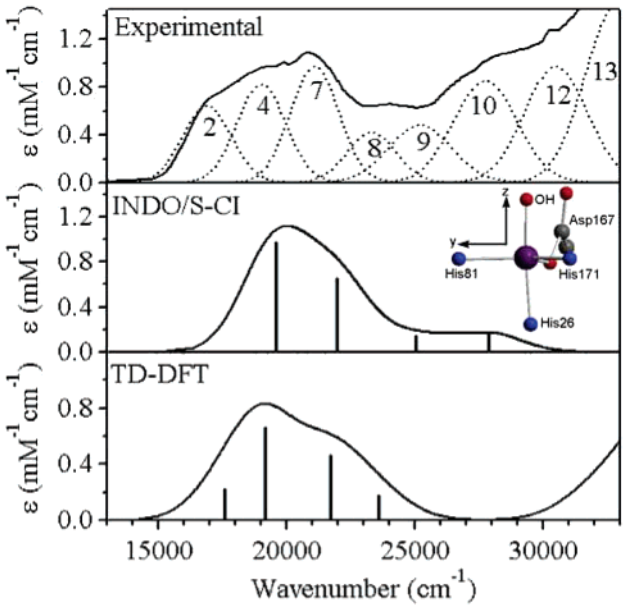

Figure 9. Top: Experimental absorption spectrum of Mn^{3+}SOD at 10 K (solid line) and corresponding Gaussian deconvolution (dotted lines). Center and bottom: Simulated absorption spectra based on INDO/S-CI and TD-DFT computations, respectively, performed on our active-site model of Mn^{3+}SOD. The four spin-allowed d → d transitions are indicated by vertical sticks. Inset: Truncated form of the Mn^{3+}SOD active-site model used for the computations. The axis system relates to the **D**-tensor orientation obtained from INDO/S-CI computations.

to the ligand orbitals. Thus, while d → d transition energies are accurately predicted by this method, LMCT transition energies, which are particularly sensitive to the energy separation between ligand-centered and metal d-based MOs, are in poor agreement with experimental data.

To find a better method for predicting electronic transition energies, time-dependent (TD) DFT computations using the B3LYP hybrid functional were performed on our active-site model of Mn^{3+}SOD.[78] While TD-DFT computations have previously been performed on hypothetical active-site models of the superoxide adducts of Mn^{2+}SOD and Fe^{2+}SOD to explore the mechanism of antiferromagnetic coupling between the superoxide ligand and the active-site metal ions,[79] to our knowledge, this method has not previously been applied to any Mn^{3+}SOD species for predicting d → d and LMCT transition energies, intensities, and polarizations. TD-DFT calculations were initially performed using our entire Mn^{3+}SOD model; however, nearly identical results were obtained for a model lacking the second-sphere Tyr34 and Gln146 residues. Thus, these residues were omitted in subsequent computations unless otherwise noted.[80] TD-DFT computations performed on our active-site model of Mn^{3+}SOD predict four d → d transitions between 17 000 and 24 000 cm^{-1} to give rise to a broad absorption envelope ($\epsilon \approx 1$ $mM^{-1}cm^{-1}$), in excellent agreement with experimental data (Figure 9). In contrast to the results of

Table 2. Metal−Ligand Bond Lengths for Six-Coordinate N_3−Mn^{3+}SOD Active Sites as Determined by X-ray Crystallography (PDB file 1MNG-L) and Partial DFT Energy Minimizations

	1MNG-L	N_3–$MnSOD^{OH}$	N_3–$MnSOD^{H2O}$
bond lengths (Å)			
Mn−N(N_2)	2.22	2.38	2.00
Mn−O_{sol}	1.95	1.80	2.28
Mn−O(Asp167)	2.25	2.14	2.00
Mn−N(His171)	2.12	2.10	2.18
Mn−N(His26)	2.12	2.12	2.26
Mn−N(His81)	2.07	2.11	2.13

INDO/S-CI computations, TD-DFT computations also predict several LMCT transitions near 30 000 cm^{-1}, in much better agreement with experimental data, where the onset of CT transitions is observed at ∼25 000 cm^{-1}. Moreover, TD-DFT computations performed on our model of Mn^{3+}SOD aligned according to the INDO/S-CI derived **D**-tensor orientation shown in Figure 9 predict the lowest energy d → d transition, which, on the basis of its energetic location and intensity, corresponds to band 2 in the experimental Mn^{3+}SOD absorption spectrum (Figure 3), to be 14% *x*-, 85% *y*-, and 1% *z*-polarized. This prediction is in excellent agreement with the experimental polarization of this band obtained from an analysis of corresponding VTVH MCD data; i.e., 21% *x*-, 73% *y*-, and 7% *z*-polarization.[37] As the TD-DFT method is successful in describing the excited-state properties of Mn^{3+}SOD, it is reasonable to assign bands 9, 10, 12, and 13 in the experimental absorption spectrum as His → Mn^{3+} and Asp^- → Mn^{3+} CT transitions on the basis of these computations. Specifically, TD-DFT computations predict two LMCT transitions from the two equatorial His residues to the Mn $3d_z^2$-based LUMO at ∼32 000 cm^{-1} and Asp^- → Mn^{3+} and His26 → Mn^{3+} CT transitions at slightly higher energies. Overall, TD-DFT computations prove to be considerably better suited than the INDO/S-CI method for predicting excited-state properties and have been used throughout the remainder of this study.

(B) Y34F N_3-Mn^{3+}SOD. A detailed spectroscopic and computational analysis of the geometric and electronic structures of the LT form of N_3−Mn^{3+}SOD is beyond the scope of this study and will therefore be presented in a separate paper.[37] Nonetheless, key results from this analysis will be briefly summarized here to facilitate comparison of active-site models of LT (six-coordinate) and RT (five-coordinate) N_3−Mn^{3+}-SOD[81] as well as to aid in the interpretation of spectroscopic data obtained for Y34F N_3−Mn^{3+}SOD.

A model of LT N_3−Mn^{3+}SOD was generated by using the X-ray structure coordinates (PDB file 1MNG-L) as a starting point for DFT geometry optimizations in which the H_3C_β groups of all first-sphere amino acids as well as all second-sphere residues not involving in the H-bond network were held fixed. Two models of LT N_3−Mn^{3+}SOD were considered that possessed either an axial OH^- (N_3−$Mn^{3+}SOD^{OH}$) or H_2O ligand (N_3−$Mn^{3+}SOD^{H2O}$); relevant structural parameters for these two

(78) TD-DFT computations performed using the Perdew−Wang pure functional yielded d → d and LMCT transition energies in poor agreement with experimental data.

(79) Carrasco, R.; Morgenstern-Badarau, I.; Cano, J. *Chem. Commun.* **2003**, 436−437.

(80) In TD-DFT computations performed for putative active-site models of N_3−Mn^{3+}SOD, the H-bond donation from Tyr34 to the azide ligand, which may be important in determining N_3^-→ Mn^{3+} CT transition energies, was accounted for by replacing the Tyr34 residue with a H_2O molecule oriented in a manner identical to the phenolic −COH group of Tyr34.

(81) Based on published thermodynamic parameters (see ref 23), there is still a fraction of six-coordinate N_3−Mn^{3+}SOD present at RT; thus, it may initially seem inappropriate to equate the RT form of N_3−Mn^{3+}SOD with five-coordinate N_3−Mn^{3+}SOD. However, the fraction of six-coordinate N_3−Mn^{3+}SOD present at RT is predicted to be very small (∼8%), as exemplified by the fact that the RT spectroscopic properties of N_3−Mn^{3+}SOD are suggestive of a five-coordinate Mn^{3+} center, thus reflecting the vast majority of five-coordinate active sites present at this temperature. Therefore, our computational models of N_3−Mn^{3+}SOD possessing a five-coordinate Mn^{3+} center are referred to as models of RT N_3−Mn^{3+}SOD.

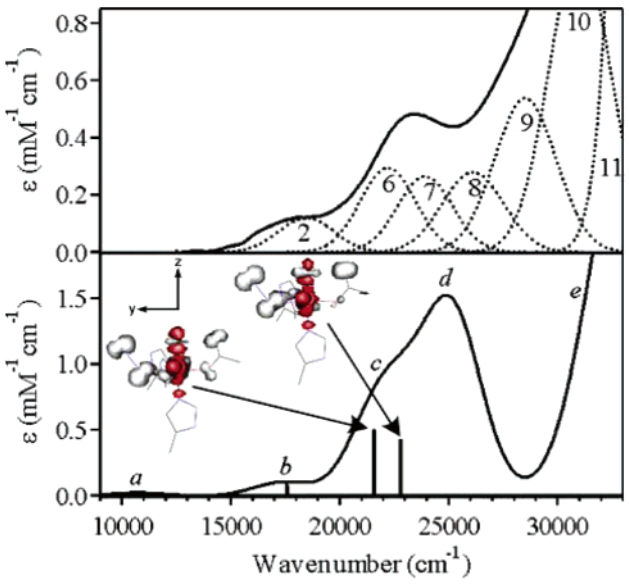

Figure 10. Top: Experimental absorption spectrum of Y34F N_3-Mn^{3+}-SOD at RT (solid line) and corresponding Gaussian deconvolution (dotted lines). Bottom: TD-DFT computed absorption spectrum for the N_3-Mn^{3+}-SOD^{OH} model. The four spin-allowed Mn^{3+} d → d transitions are indicated by vertical sticks. Inset: EDDMs of the two highest energy d → d transitions predicted for $N_3-Mn^{3+}SOD^{OH}$. Red and gray denote gain and loss of electron density, respectively.

models after geometry optimization are given in Table 2. To estimate the acidity of the axial solvent ligand of six-coordinate $N_3-Mn^{3+}SOD$, a previously employed method was used to compute a ΔpK value between $N_3-Mn^{3+}SOD$ and $Mn^{2+}SOD$, the latter of which was chosen as a reference model because it possesses the same overall charge as $N_3-Mn^{3+}SOD$.[37] These computations revealed that the axial solvent ligand of N_3-Mn^{3+}-SOD is more acidic than that of $Mn^{2+}SOD$ by ~21 pH units. As previous DFT/electrostatics calculations by Noodleman and co-workers led to the proposal that the absolute pK value of the axial solvent ligand of $Mn^{2+}SOD$ is ~10−18, our results strongly suggest that $N_3-Mn^{3+}SOD$ binds OH^- rather than H_2O in the axial position at neutral pH. In further support of this hypothesis, the TD-DFT computed absorption spectrum of $N_3-Mn^{3+}SOD^{OH}$ bears a striking resemblance to the experimental spectrum of six-coordinate Y34F $N_3-Mn^{3+}SOD$ (Figure 10). In contrast, the TD-DFT computed $N_3-Mn^{3+}SOD^{H2O}$ absorption spectrum is dramatically different, exhibiting an intense ($\epsilon \approx 4$ mM^{-1} cm^{-1}) feature at ~17 500 cm^{-1} that has no counterpart in the experimental spectrum.

In light of the striking spectral similarities between LT $N_3-Mn^{3+}SOD$ and Y34F $N_3-Mn^{3+}SOD$ (vide supra), it is reasonable to use the TD-DFT results obtained for $N_3-Mn^{3+}SOD^{OH}$ as a basis for interpreting the spectroscopic properties of Y34F $N_3-Mn^{3+}SOD$. Consequently, band 2 in the experimental spectrum of Y34F $N_3-Mn^{3+}SOD$ (Figure 10), corresponding to feature *b* in the TD-DFT computed spectrum, may be assigned as the Mn $3d_{xz} \rightarrow 3d_z^2$ transition that is considerably mixed with an $N_3^- \rightarrow Mn^{3+}$ CT transition, thus rationalizing the enhancement of $\nu_s(N_3)$ in this region (Figure 8). Bands 6 and 7 are assigned as Mn $3d_{xy} \rightarrow 3d_z^2$ and $3d_{yz} \rightarrow 3d_z^2$ transitions, respectively, where both donor MOs contain significant contributions from the N_3^- π nonbonding (π^{nb}) orbitals. Examination of electron density difference maps (EDDMs) for these transitions (see Figure 10, bottom inset) reveals that in addition to a generalredistribution of electron density at the Mn^{3+} center (reflecting the d → d character of these transitions), the corresponding excited states are stabilized by transfer of electron density from the N_3^- π^{nb}-based MOs to the Mn^{3+} 3d-derived donor MOs. Importantly, these EDDMs reveal symmetric loss of electron density from the terminal nitrogens of the N_3^- ligand, suggesting that excitation in resonance with bands 6 and 7 should give rise to symmetric distortions of this ligand, thus providing an intuitively appealing explanation for the selective RR enhancement of $\nu_s(N_3)$ over $\nu_{as}(N_3)$ in this region (Figure 8).

TD-DFT computations performed on $N_3-Mn^{3+}SOD^{OH}$ also reveal that multiple $N_3^- \rightarrow Mn^{3+}$ CT transitions, possessing varying degrees of His → Mn^{3+} and $Asp^- \rightarrow Mn^{3+}$ CT character, give rise to bands *d* and *e*. Specifically, bands *d* and *e* (Figure 10, bottom) contain contributions from $N_3^- \rightarrow Mn^{3+}$ CT transitions where the acceptor MOs are the Mn^{3+} t_{2g}- and e_g-derived MOs (using symmetry labels of the parent O_h point group), respectively, and LMCT transitions that give rise to band *e* are predicted to be roughly twice as intense as those giving rise to band *d*. On the basis of these results, bands 8 and 9 of Y34F $N_3-Mn^{3+}SOD$, which exhibit moderate absorption intensities, are assigned as $N_3^- \rightarrow Mn^{3+}$ t_{2g}-type CT transitions, whereas the more intense bands 10 and 11 are attributed to $N_3^- \rightarrow Mn^{3+}$ e_g-type CT transitions. These assignments are fully consistent with our absorption, CD, and MCD studies of $N_3-Mn^{3+}SOD$ and Y34F $N_3-Mn^{3+}SOD$ (vide supra), which also suggest that all near-UV features above ~25 000 cm^{-1} are due to $N_3^- \rightarrow Mn^{3+}$ CT transitions.

(C) RT $N_3-Mn^{3+}SOD$. Whittaker and Whittaker have shown that the RT state of $N_3-Mn^{3+}SOD$ represents a local enthalpy minimum that is ~5 kcal/mol above the global minimum defined by the LT form of $N_3-Mn^{3+}SOD$ (specifically, $\Delta H = 5$ and 6.3 kcal/mol for $N_3-Mn^{3+}SOD$ from *E. coli* and *T. thermophilus*, respectively).[23,24] This enthalpy difference provided one criterion that we have used to evaluate hypothetical active-site models of RT $N_3-Mn^{3+}SOD$; i.e., for a model to be deemed reasonable, its total energy must be ~5 kcal/mol higher than that of our experimentally validated $N_3-Mn^{3+}SOD^{OH}$ model of LT $N_3-Mn^{3+}SOD$[37] described above. The second criterion used to evaluate these five-coordinate $N_3-Mn^{3+}SOD$ models was that their TD-DFT computed absorption spectra (in particular the splitting pattern of the d → d excited states) must resemble the experimental spectrum of RT $N_3-Mn^{3+}SOD$.

While our spectroscopic and computational data indicate that the axial solvent ligand of LT $N_3-Mn^{3+}SOD$ is OH^- rather than H_2O,[37] it may be argued that the RT form of N_3-Mn^{3+}-SOD, which has a lower coordination number of the Mn^{3+} ion, possesses an elevated pK. Therefore, in generating hypothetical active-site models for RT $N_3-Mn^{3+}SOD$, we have considered both protonation states of the axial solvent ligand. Models of RT $N_3-Mn^{3+}SOD$ were generated by distorting the geometry of the six-coordinate $N_3-Mn^{3+}SOD$ active site provided by X-ray structure data to promote either solvent ($N_3-Mn^{3+}SOD$-(−OH) and $N_3-Mn^{3+}SOD(-H_2O)$), Asp167 ($N_3-Mn^{3+}SOD^{OH}$-(−Asp) and $N_3-Mn^{3+}SOD^{H2O}(-Asp)$), or N_3^- (N_3-Mn^{3+}-$SOD^{OH}(-N_3)$) dissociation from the Mn^{3+} center. These models were subsequently refined using constrained DFT energy minimizations (Figure 11, right and Table 3), where the H_3C_β groups of the first-sphere residues as well as all second-sphere

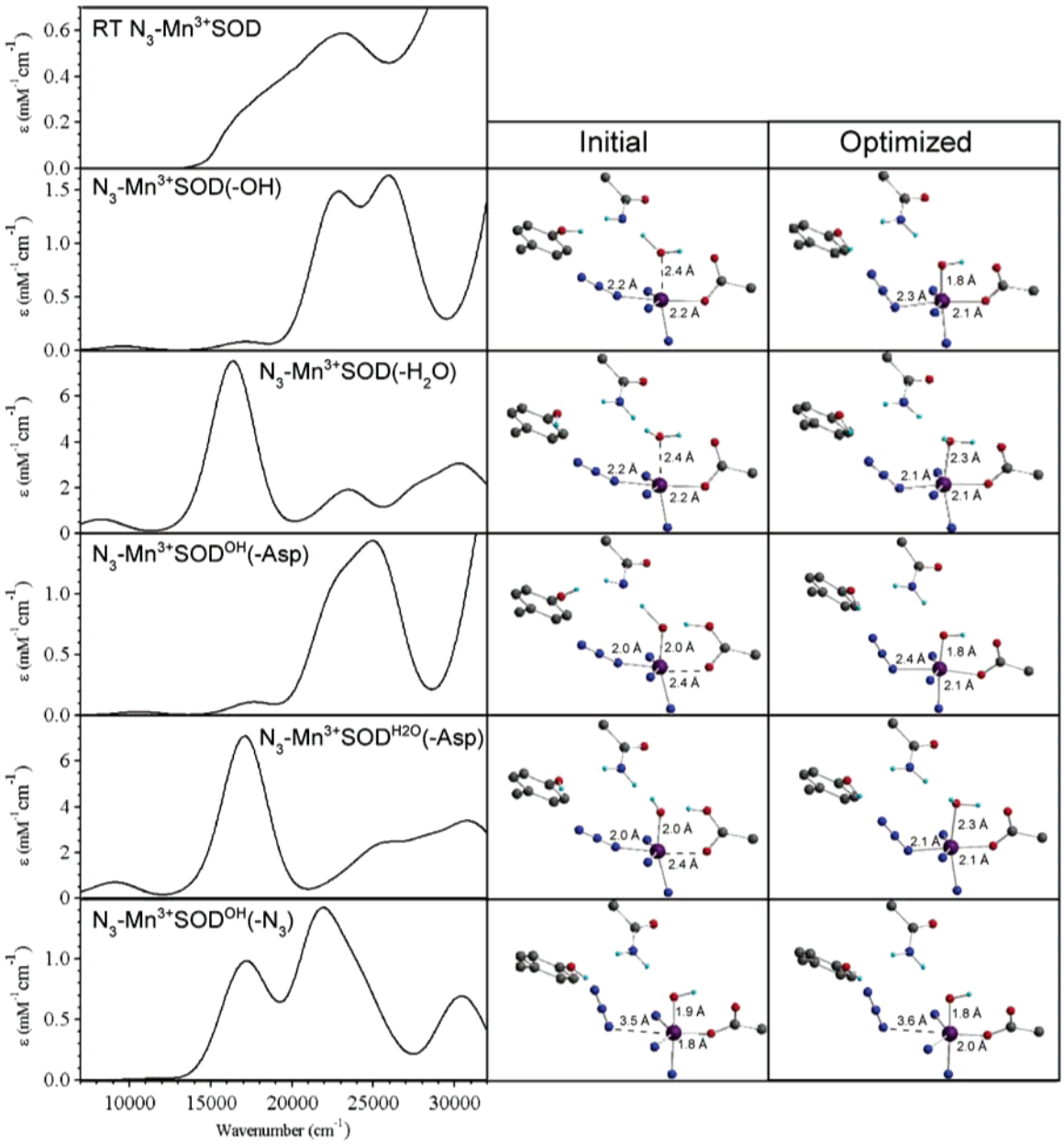

Figure 11. Experimental absorption spectrum of RT $N_3-Mn^{3+}SOD$ (top left) and predicted absorption spectra (left) based on TD-DFT computations performed on the geometry-optimized hypothetical active-site models of RT $N_3-Mn^{3+}SOD$ shown on the far right. The structures of these models, shown before and after geometry optimization, have been truncated so as to show only the coordinating N atoms of the His residues and the H atoms involved in the conserved H-bond network. Relevant bond lengths before and after geometry optimization are given.

Table 3. Metal−Ligand Bond Lengths for DFT Geometry-Optimized Active-Site Models of RT $N_3-Mn^{3+}SOD$

	N_3–MnSOD(–OH)	N_3–MnSOD^{OH}(–Asp)	N_3–MnSOD(–H_2O)	N_3–MnSOD^{H2O}(–Asp)	N_3–MnSOD^{OH}(–N_3)
bond lengths (Å)					
Mn−N(N_2)	2.30	2.37	2.12	2.08	3.58
Mn−O_{sol}	1.81	1.81	2.26	2.33	1.81
Mn−O(Asp167)	2.11	2.14	2.14	2.07	1.98
Mn−N(His171)	2.13	2.09	2.13	2.17	2.07
Mn−N(His26)	2.13	2.12	2.20	2.20	2.06
Mn−N(His81)	2.12	2.10	2.10	2.13	2.04

residues not involved in the H-bond network (Figure 1) were held fixed. Note that $N_3-Mn^{3+}SOD(-OH)$, $N_3-Mn^{3+}SOD^{OH}(-Asp)$, and $N_3-Mn^{3+}SOD^{OH}(-N_3)$ contain the same overall protonation state as $N_3-Mn^{3+}SOD^{OH}$, whereas $N_3-Mn^{3+}SOD(-H_2O)$ and $N_3-Mn^{3+}SOD^{H2O}(-Asp)$ possess an additional proton. As computed energies can be compared only for systems that possess the same number and type of atoms, the ΔH values for $N_3-Mn^{3+}SOD(-H_2O)$ and $N_3-Mn^{3+}SOD^{H2O}(-Asp)$ have been determined using $N_3-Mn^{3+}SOD^{H2O}$ (Table 2) as a reference point.

$N_3-Mn^{3+}SOD(-OH)$ and $N_3-Mn^{3+}SOD(-H_2O)$ converged to geometries that are 2.5 and 13.3 kcal/mol higher in energy

than $N_3-Mn^{3+}SOD^{OH}$ and $N_3-Mn^{3+}SOD^{H2O}$, respectively. As the relative energy of $N_3-Mn^{3+}SOD(-H_2O)$ is much greater than that of $N_3-Mn^{3+}SOD(-OH)$, the pK of $N_3-Mn^{3+}SOD(-H_2O)$ must be significantly lower than that of $N_3-Mn^{3+}SOD^{H2O}$, and, thus, the axial solvent ligand of $N_3-Mn^{3+}SOD(-H_2O)$ is predicted to be even more acidic (pK < 0). Table 3 and Figure 11 reveal that after geometry optimization, the axial solvent ligand of both the $N_3-Mn^{3+}SOD(-OH)$ and the $N_3-Mn^{3+}SOD(-H_2O)$ models reassociates with the Mn^{3+} ion to generate a six-coordinate active site, suggesting that dissociation of the solvent ligand is not likely to be the source of the thermochromism observed for $N_3-Mn^{3+}SOD$. In support of this conclusion, the corresponding TD-DFT computed absorption spectra exhibit a "red-band" at ~10 000 cm^{-1}, in clear disagreement with the experimental absorption spectrum of RT $N_3-Mn^{3+}SOD$ (Figure 11) that lacks any discernible features at energies <15 000 cm^{-1}.

The energies of the DFT optimized $N_3-Mn^{3+}SOD^{OH}(-Asp)$ and $N_3-Mn^{3+}SOD^{H2O}(-Asp)$ models are 3.4 and 10.6 kcal/mol higher than those of $N_3-Mn^{3+}SOD^{OH}$ and $N_3-Mn^{3+}SOD^{H2O}$, respectively, with the former value being compatible with the experimental ΔH value. However, in each case the Mn−O(Asp167) bond length, initially set to 2.4 Å, decreased dramatically by ~0.3−0.4 Å upon geometry optimization to generate a six-coordinate Mn^{3+} active-site ion (Table 3, Figure 11). Consequently, the TD-DFT computed absorption spectra for these two models also exhibit a d → d transition in the NIR region, revealing that $N_3-Mn^{3+}SOD^{OH}(-Asp)$ and $N_3-Mn^{3+}SOD^{H2O}(-Asp)$ are unacceptable models for RT $N_3-Mn^{3+}SOD$.

During geometry optimization of the $N_3-Mn^{3+}SOD^{OH}(-N_3)$ model, the azide ligand did not approach the Mn^{3+} ion but instead retained a strong H-bond with Tyr34 (Figure 11, right). As $N_3-Mn^{3+}SOD^{OH}(-N_3)$ is only 6.2 kcal/mol higher in energy than $N_3-Mn^{3+}SOD^{OH}$, it is a suitable model for RT $N_3-Mn^{3+}SOD$ on the basis of its relative energy. TD-DFT calculations on $N_3-Mn^{3+}SOD^{OH}(-N_3)$ predict four d → d transitions in the visible spectral region that are largely responsible for the two closely spaced features at ~17 000 and 22 000 cm^{-1} in the computed absorption spectrum (Figure 11). Importantly, no d → d transitions are predicted in the NIR region, further distinguishing this model from all other $N_3-Mn^{3+}SOD$ models tested. On the basis of this excellent reproduction of the experimental d → d excited-state splitting pattern of RT $N_3-Mn^{3+}SOD$, the $N_3-Mn^{3+}SOD^{OH}(-N_3)$ model is the only reasonable active-site model of RT $N_3-Mn^{3+}SOD$.

4. Discussion

It has been known for almost a decade that the crystallographically characterized six-coordinate $N_3-Mn^{3+}SOD$ active site[12] converts to a five-coordinate form as temperature is increased;[23,24] however, the ligand that dissociates in this conversion has remained unidentified. In this study, we have used a variety of spectroscopic and computational techniques to explore the geometric and electronic properties of the active sites of resting $Mn^{3+}SOD$ and Y34F $N_3-Mn^{3+}SOD$ from *E. coli*, thereby developing a suitable framework for the characterization of the structurally ill-defined active site of RT $N_3-Mn^{3+}SOD$. Below, key findings from these studies and their implications with respect to second-sphere tuning of substrate (analog)/active site interactions are discussed.

Six-Coordinate N_3-Mn^{3+}SOD. Our absorption, CD, MCD, and RR studies reveal that azide binds to Y34F $Mn^{3+}SOD$ to form a *temperature-independent* six-coordinate N_3-Mn^{3+} complex that possesses geometric and electronic structures nearly identical with those of LT $N_3-Mn^{3+}SOD$, in support of previous proposals based on the similarity of the absorption spectra of these two species.[23] In addition to eliminating the thermochromism associated with the N_3-Mn^{3+} active site, substitution of the second-sphere Tyr34 residue with Phe also decreases the dissociation constant of azide by nearly 5-fold (K_d = 7.2 and 1.6 mM for WT and Y34F $Mn^{3+}SOD$, respectively).[27] It has been previously proposed that the increased affinity for N_3^- of Y34F $Mn^{3+}SOD$ relative to WT $Mn^{3+}SOD$ may be attributed to the relaxation of steric constraints in the substrate funnel (i.e., the cavity defined by Tyr34, His30 and the Mn^{3+} center,[82] Figure 1) and/or increased charge on the metal center accompanying this substitution.[83] Indeed, our RR results (Figure 7) reveal a greater flexibility of the N_3-Mn^{3+} unit in the variant species, providing experimental evidence for a less sterically constrained azide adduct. Alternatively, the observation that Y34F $Mn^{3+}SOD$ binds fluoride less tightly than $Mn^{3+}SOD$ (K_d = 25 and 75 mM for WT and Y34F $Mn^{3+}SOD$, respectively)[27] argues against increased positive charge on the Mn^{3+} ion in this variant, as otherwise the relative affinities for fluoride should be reversed. These results suggest that in the native enzyme Tyr34 directly interacts with azide, most likely through donation of a H-bond to the terminal nitrogen atom of coordinated azide, as suggested by X-ray studies on *T. thermophilus* $N_3-Mn^{3+}SOD$.[12] The mechanistic significance of this result is difficult to assess, as it is unclear whether the orientation of bound superoxide, which is significantly smaller than azide, could be similarly influenced by Tyr34. However, while Y34F and WT MnSOD exhibit nearly identical catalytic activities,[27,83] the Y34F substitution has been shown to decrease the turnover number of human MnSOD (i.e., k_{cat}) by an order of magnitude without affecting k_{cat}/K_m[84] and to increase the susceptibility of the active-site Mn ion to product-inhibition,[85] demonstrating that Tyr34 does play an important role in superoxide dismutation (vide infra).

Nature of RT N_3-Mn^{3+}SOD. A detailed analysis of our spectroscopic data obtained for RT $N_3-Mn^{3+}SOD$ reveals that this complex exhibits a d → d splitting pattern nearly identical to that observed for resting $Mn^{3+}SOD$ (Figure 6), suggesting that the Mn^{3+} coordination geometry for these systems is similar. DFT geometry optimizations of hypothetical active-site models of RT $N_3-Mn^{3+}SOD$ with dissociated solvent or Asp167 ligands consistently converged to six-coordinate Mn^{3+} systems and, consequently, to the appearance of a NIR d → d transition in the corresponding TD-DFT computed absorption spectra (the "red-band") that has no counterpart in the experimental spectrum (Figure 11). In contrast, geometry optimization of a hypothetical active-site model with dissociated azide preserved a five-coordinate Mn^{3+} center, and TD-DFT computations performed on this model predict an absorption spectrum bearing a high

(82) Hunter, T.; Ikebukuro, K.; Bannister, W. H.; Bannister, J. V.; Hunter, G. J. *Biochemistry* **1997**, *36*, 4925−4933.
(83) Edwards, R. A.; Whittaker, M. M.; Whittaker, J. W.; Baker, E. N.; Jameson, G. B. *Biochemistry* **2001**, *40*, 15−27.
(84) Guan, Y.; Hickey, M. J.; Borgstahl, G. E. O.; Hallewell, R. A.; Lepock, J. R.; O'Connor, D.; Hsieh, Y. S.; Nick, H. S.; Silverman, D. N.; Tainer, J. A. *Biochemistry* **1998**, *37*, 4722−4730.
(85) Lévêque, V. J.-P.; Vance, C. K.; Nick, H. S.; Silverman, D. N. *Biochemistry* **2001**, *40*, 10 586−10 591.

resemblance to the experimental spectrum of RT N_3-Mn^{3+}-SOD. Thus, on the basis of these data alone, it would seem reasonable to conclude that RT N_3-Mn^{3+}SOD contains an azide molecule that is not bound to the Mn^{3+} ion ($Mn\cdots N(N_2)$ distance of 3.6 Å, Table 3) but instead H-bonds with Tyr34.

However, this conclusion initially appears to conflict with our RR data obtained for N_3-Mn^{3+}SOD at 273 K, which clearly reveal the presence of vibrational features associated with a N_3-Mn^{3+} unit similar to that of LT N_3-Mn^{3+}SOD (Figure 7 and Table 1). On the basis of published thermodynamic parameters obtained from a van't Hoff analysis of variable-temperature absorption data, the equilibrium constant for the interconversion between the LT and RT forms of N_3-Mn^{3+}SOD (LT$\leftrightarrow$RT) is $K_{eq} = 6.3$ at 273 K.[23] As this equilibrium describes a dynamic process, the LT and RT forms of N_3-Mn^{3+}SOD will be rapidly interconverting at 273 K. Importantly, on the time scale of RR experiments ($\sim 10^{-14}$ s), these distinct species should be sufficiently long-lived such that vibrations associated with the N_3-Mn^{3+} unit of the six-coordinate fraction (~15%) that is still present at this temperature can be observed in RR experiments performed at 273 K. Similarly, the absorption spectrum obtained at ~295 K represents the sum of contributions from five-coordinate (~92%) and six-coordinate (~8%) forms that are in equilibrium; thus, an average spectrum (albeit mainly reflecting the five-coordinate fraction) due to this ensemble is observed.

Our proposal that unligated N_3^- is stabilized by a H-bonding interaction with Tyr34 in RT N_3-Mn^{3+}SOD is supported by the observation that substitution of Tyr34 to Phe abolishes the thermochromism of N_3-Mn^{3+}SOD.[27] Replacement of the polar Tyr34 residue with a hydrophobic Phe residue eliminates the ability of azide to develop a H-bond with residue 34 without providing enough space for the azide ligand to reorder and H-bond with another second-sphere residue (e.g., His30). It is somewhat puzzling, then, that the absorption spectrum of Y34A N_3-Mn^{3+}SOD, where the Tyr34 residue has been replaced with Ala, does not appear to reflect 100% six-coordinate N_3-Mn^{3+}-SOD.[83] However, azide binding to Y34A Mn^{3+}SOD was not examined in detail, and it is not clear, for example, whether the azide adduct of this variant is thermochromic or not. Interestingly, absorption spectra reported for the H30A and H30N variants of Mn^{3+}SOD in the presence of azide appear slightly altered relative to that of RT N_3-Mn^{3+}SOD,[86] indicating that His30 might also play a role in defining the putative second-sphere binding pocket for azide. Clearly, a more detailed study of the Y34A, H30A, and H30N N_3-Mn^{3+}SODs utilizing variable-temperature absorption and LT MCD spectroscopies to further examine the influence of these substitutions on azide binding is needed. If these variant proteins are in fact thermochromic, then such studies would potentially also prove useful in determining how *E. coli* and *T. thermophilus* Mn^{3+}SOD are able to selectively tune their active-site properties to achieve thermochromic transition temperatures that differ by ~80 K.[23,24]

While some substitutions of Tyr34 and His30 still allow N_3^- to access the Mn^{3+} ion, substitution of Gln146, a residue involved in H-bonding with Tyr34 and coordinated solvent (Figure 1), to His or Leu has been shown to prevent azide binding.[83] This observation may initially be interpreted as indicating that the thermochromic transition of the native N_3-Mn^{3+}SOD species involves axial solvent ligand dissociation at RT, as removal of the strong H-bond donor Gln146 would no longer allow for stabilization of the dissociated solvent molecule. However, as shown by Edwards et al.,[83] substitution of Gln146 to His or Leu results in a drastic shift in the position of Tyr34. Importantly, this residue moves closer to the Mn^{3+} ion (~0.5 Å) and His30 (~1 Å), thereby greatly restricting access to the Mn^{3+} active site.[83] Thus, the lack of azide binding of the Q146H and Q146L variants does not conflict with our model of thermochromism, but in fact provides further evidence for the importance of Tyr34 in modulating the interaction between azide and the active site of Mn^{3+}SOD. As azide presumably coordinates to the Mn^{2+} center of reduced Mn^{2+}SOD,[22,25] EPR studies of azide-treated Q146H or Q146L Mn^{2+}SOD should prove useful in determining if the lack of azide binding to the oxidized Mn^{3+} ion indeed arises from restricted access to the active site. It should be noted that, as mentioned above, results obtained using azide do not necessarily apply to substrate superoxide, as the latter is roughly 50% smaller than azide. Indeed, while substitution of His30 to Val in human MnSOD has also been shown to limit access to the active site, resulting in a Mn^{3+} ion that does not appear to ligate azide at RT,[87] the H30V variant still displays significant product inhibition through formation of an inner-sphere complex. Hence, superoxide, unlike azide, does have access to the Mn center of H30V MnSOD.[87]

Visual Probe of Solvent Ligand Protonation State. It is noteworthy that the TD-DFT predicted absorption spectra for $N_3-Mn^{3+}SOD(-H_2O)$ and $N_3-Mn^{3+}SOD^{H2O}(-Asp)$, models that both possess an axial H_2O ligand, exhibit an intense ($\epsilon \approx 6\ mM^{-1}cm^{-1}$) feature at ~16 000 cm^{-1} (Figure 11) due to a LMCT transition from an N_3^- π^{nb}-based MO to the Mn^{3+} $3d_{x^2-y^2}$-derived LUMO. In contrast, TD-DFT computed absorption spectra of all N_3-Mn^{3+}SOD models with a OH^- ligand (i.e., $N_3-Mn^{3+}SOD^{OH}$, $N_3-Mn^{3+}SOD(-OH)$, $N_3-Mn^{3+}SOD^{OH}(-Asp)$, and $N_3-Mn^{3+}SOD^{OH}(-N_3)$) lack any intense features at energies <22 000 cm^{-1} (Figures 10 and 11). Insight into the origin of these different spectral properties is provided by the DFT computed bonding descriptions of $N_3-Mn^{3+}SOD(-H_2O)$ and $N_3-Mn^{3+}SOD(-OH)$, used here as representative examples of N_3-Mn^{3+}SOD models with axial H_2O and OH^- ligand, respectively. As shown in Figure 12, the identity of the axial solvent ligand dictates the nature of the Mn 3d-based LUMO. Specifically, the presence of a H_2O ligand leads to an elongation along the $O_{sol}-Mn-N(His26)$ axis, resulting in a Mn $3d_{x^2-y^2}$-derived LUMO (Figure 12, top left). Conversely, the presence of an axial OH^- ligand gives rise to a compression along this axis, yielding a Mn $3d_{z^2}$-derived LUMO (Figure 12, bottom left). As the intensity of LMCT transitions is governed by the amount of ligand orbital character in the corresponding donor and acceptor MOs,[88,89] it is not surprising that excitation from an N_3^- π^{nb}-based MO to the Mn^{3+} $3d_{x^2-y^2}$-derived LUMO of $N_3-Mn^{3+}SOD(-H_2O)$ gives rise to an intense feature in the visible region of the TD-DFT computed absorption spectrum (Figure 11). While a corresponding transition is also expected to occur for $N_3-Mn^{3+}SOD(-OH)$, the Mn $3d_{x^2-y^2}$-derived acceptor MO

(86) Edwards, R. A.; Whittaker, M.; Whittaker, J.; Baker, E. N.; Jameson, G. B. *Biochemistry* **2001**, *40*, 4622−4632.
(87) Hearn, A. S.; Stroupe, M. E.; Cabelli, D. E.; Ramilo, C. A.; Luba, J. P.; Tainer, J. A.; Nick, H. S.; Silverman, D. N. *Biochemistry* **2003**, *42*, 2781−2789.
(88) Solomon, E. I. *Comments Inorg. Chem.* **1984**, *3*, 255.
(89) Baldwin, M. J.; Root, D. E.; Pate, J. E.; Fujisawa, K.; Kitajima, N.; Solomon, E. I. *J. Am. Chem. Soc.* **1992**, *114*, 10 421−10 431.

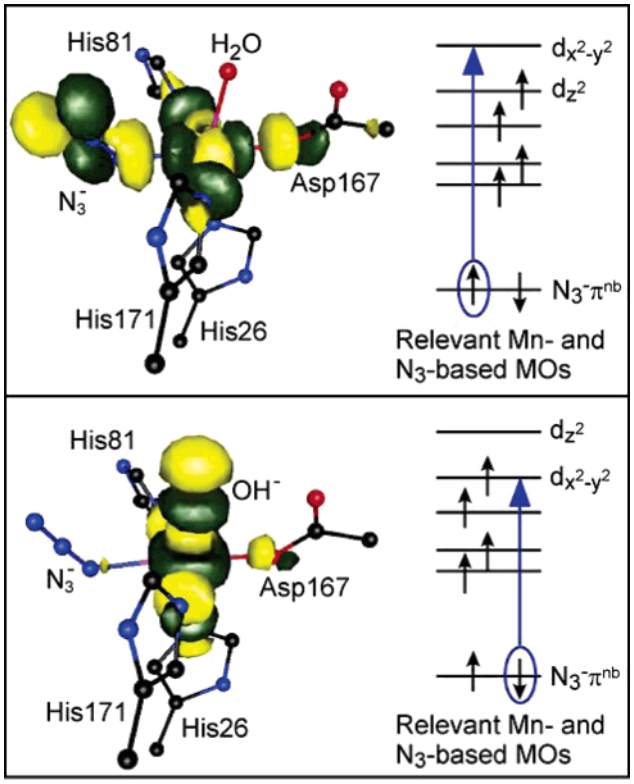

Figure 12. Contour plots of the Mn^{3+} 3d-based natural LUMOs (left) and qualitative MO energy level diagram (right) for $N_3-Mn^{3+}SOD(-H_2O)$ (top) and $N_3-Mn^{3+}SOD(-OH)$ (bottom). The blue arrows on the right indicate the intense N_3^- $\pi^{nb} \rightarrow Mn^{3+}$ $3d_{x^2-y^2}$ CT transition for each species.

of this species is now singly occupied in the ground state (Figure 12, bottom). Thus, the intense $N_3^- \rightarrow Mn^{3+}$ CT transition predicted for $N_3-Mn^{3+}SOD(-OH)$ formally results in an excited $S = 3/2$ Mn^{2+} ion, as opposed to a ground state $S = 5/2$ Mn^{2+} ion as predicted for $N_3-Mn^{3+}SOD(-H_2O)$, thus blue-shifting this transition by $\sim$20 000 cm^{-1} into the UV region. A general rule can therefore be formulated, stating that whenever the unoccupied Mn 3d-based MO lies along the $(N_2)N-Mn-O(Asp167)$ axis, an intense $N_3^- \rightarrow Mn^{3+}$ CT transition will occur in the visible spectral region, as the corresponding excited state energy has no contribution from spin-pairing on the transiently formed Mn^{2+} ion. Alternatively, the spin-pairing energy associated with an $S = 3/2$ Mn^{2+} excited state, which results when the Mn 3d-based MO oriented along the $(N_2)N-Mn-O(Asp167)$ axis is singly occupied in the ground state, is expected to shift this transition deep into the near-UV region. It should be noted, however, that this rule is not without a caveat; namely, if one of the two metal−ligand bonds coincident with the $(N_2)N-Mn-O(Asp167)$ axis is unusually short, then the Mn 3d-based MO that is oriented along this axis may be sufficiently destabilized to shift the intense $N_3^- \rightarrow Mn^{3+}$ CT transition into the near-UV spectral region even if the acceptor MO is unoccupied in the ground state.

Mechanistic Implications. This general rule regarding the solvent ligand protonation state may have implications with respect to the geometric structure of the product-inhibited form of MnSOD (a putative peroxo-Mn^{3+}SOD species) that is formed when Mn^{2+}SOD is treated with superoxide[90] or when Mn^{3+}-SOD is treated with hydrogen peroxide.[91] Intriguingly, the absorption spectrum reported for this dead-end complex is similar to that of N_3-Mn^{3+}SOD at LT.[23,90,91] On the basis of this qualitative rule and our TD-DFT computed absorption spectra for N_3-Mn^{3+}SOD species, it is tempting to speculate that the product-inhibited complex possesses a OH^- rather than a H_2O ligand in the axial position, as the latter would force the Mn-based LUMO to be oriented in the equatorial plane, potentially resulting in an intense, low-energy LMCT transition (in obvious disagreement with experimental data). On the basis of similar considerations, it appears unlikely that Asp167 dissociates upon formation of the dead-end complex, as dissociation of this ligand would be expected to similarly orient the Mn-based LUMO along the peroxo-Mn axis, also giving rise to an intense LMCT transition in the visible spectral region. While the spectroscopic similarities between the dead-end complex and LT N_3-Mn^{3+}SOD suggest that the former is a hydroperoxo-Mn^{3+} adduct, resulting from electron transfer from Mn^{2+} to $O_2^{\cdot -}$ with concomitant H^+ transfer from coordinated H_2O to the *terminal* O atom of the nascent peroxo ligand, further studies are needed to test this hypothesis. Given the success of the TD-DFT method at reproducing key features of the experimental absorption spectra of Mn^{3+}SOD species, this computational method appears particularly well suited to evaluate viable models of the dead-end complex.

Another important result from our studies of RT N_3-Mn^{3+}-SOD is that the endogenous ligands of Mn^{3+}SOD are not, as previously suggested, labile and therefore should remain coordinated during the catalytic cycle, thus implying that formation of a symmetric side-on peroxo-Mn^{3+} species is unlikely. In stark contrast, the substrate (analog) binding site of Mn^{3+}SOD seems quite labile, as at RT N_3^- appears to fluctuate between being ligated to the Mn^{3+} ion or H-bonded to the second-sphere Tyr34 residue. Intriguingly, the lability of this open coordination site is affected by the identities of both the metal ion, (note that Fe^{3+} substituted MnSOD binds azide at room temperature to form a six-coordinate adduct[32]) and the second-sphere amino acid residues (e.g., substitution of Tyr34 to Phe generates a six-coordinate N_3-Mn^{3+} adduct at all temperatures).[27] Thus, in addition to ensuring rapid proton transfer to nascent product during substrate reduction (eq 2b), second-sphere residues such as Tyr34 also appear to play a key role in modulating the kinetics and thermodynamics of substrate (analog) binding to, and dissociation from, the active-site Mn^{3+} ion. Indeed, kinetic studies performed by Silverman and co-workers have shown that substitutions of Tyr34 and His30 (among others) drastically affect the kinetics of superoxide dismutation, especially by decreasing the rate of reaction with superoxide (eq 2) and decreasing the rate of decay of the product-inhibited complex.[84,87,91,92] Therefore, the lability of the substrate (analog) binding site of Mn^{3+}SOD appears to be finely tuned by second-sphere amino acid residues to achieve optimal catalytic turnover under physiological conditions.

Acknowledgment. T. A. J. thanks the University of Wisconsin Biophysics Training Grant for financial support. T. C. B. thanks the University of Wisconsin and NIH (GM 64631)

(90) Bull, C.; Niederhoffer, E. C.; Yoshida, T.; Fee, J. A. *J. Am. Chem. Soc.* **1991**, *113*, 4069−4076.
(91) Hearn, A. S.; Tu, C. K.; Nick, H. S.; Silverman, D. N. *J. Biol. Chem.* **1999**, *274*, 24457−24460.
(92) Hearn, A. S.; Stroupe, M. E.; Cabelli, D. E.; Lepock, J. R.; Tainer, J. A.; Nick, H. S.; Silverman, D. N. *Biochemistry* **2001**, *40*, 12 051−12 058.

for financial support and acknowledges Dr. Frank Neese (MPI Mülheim) for providing a free copy of ORCA and for useful discussions. A.-F. M. acknowledges financial support by N. S. F. (MCB 0129599) and KSEF (172-RDE−002).

Supporting Information Available: Experimental parameters obtained from a Gaussian deconvolution of absorption, CD, and MCD data obtained for resting Mn^{3+}SOD, Y34F N_3−Mn^{3+}-SOD, LT N_3−Mn^{3+}SOD, and RT N_3−Mn^{3+}SOD (Tables S12−14), absorption, CD, and MCD data obtained for Y34F Mn^{3+}SOD (Figure S1), Gaussian deconvolutions of absorption and CD data obtained for RT Mn^{3+}SOD (Figure S2 and Table S15), resonance Raman excitation profile data for the phenyl ring breathing mode (Figure S3), 77 K resonance Raman spectra of N_3−Mn^{3+}SOD and Y34F N_3−Mn^{3+}SOD (Figure S4), and Cartesian coordinates for all computational models (Tables S1-S11). This material is available free of charge via the Internet at http://pubs.acs.org.

JA0482583